

Special Section:

Years of the Maritime Continent

Key Points:

- Volume, heat and freshwater transports through Karimata Strait from 1993 to 2017 are estimated based on in situ and satellite observations
- Karimata Throughflow shows a strong seasonal cycle driven by monsoon and weak interannual variation that is less correlated to Indian Ocean Dipole and El Niño-Southern Oscillation
- A significant decrease in freshwater transport into Indonesian seas may influence the decadal enhancement of the Indonesian Throughflow

Supporting Information:

- Supporting Information S1

Correspondence to:

Z. X. Wei and S. J. Li,
weizx@fio.org.cn;
lisj@fio.org.cn










Citation:

Xu, T. F., Wei, Z. X., Susanto, R. D., Li, S. J., Wang, Y. G., Wang, Y., et al. (2021). Observed water exchange between the South China Sea and Java Sea through Karimata Strait. *Journal of Geophysical Research: Oceans*, 126, e2020JC016608. <https://doi.org/10.1029/2020JC016608>

Received 18 JUL 2020

Accepted 13 JAN 2021

Observed Water Exchange Between the South China Sea and Java Sea Through Karimata Strait

T. F. Xu^{1,2,3} , Z. X. Wei^{1,2,3} , R. D. Susanto^{4,5} , S. J. Li^{1,2,3} , Y. G. Wang^{1,2,3} , Y. Wang^{1,6}, X. Q. Xu^{1,2,3} , T. Agustiadi⁷ , M. Trenggono⁸ , B. Sulisty⁹, A. Setiawan⁷, A. Kuswardani⁷, and G. H. Fang^{1,2,3} 

¹First Institute of Oceanography, Ministry of Natural Resources of China, Qingdao, China, ²Laboratory for Regional Oceanography and Numerical Modeling, Pilot National Laboratory for Marine Science and Technology (Qingdao), Qingdao, China, ³Key Laboratory of Marine Science and Numerical Modeling, Ministry of Natural Resources, Qingdao, China, ⁴Department of Atmospheric and Oceanic Science, University of Maryland, College Park, MD, USA, ⁵Faculty of Earth Sciences and Technology, Bandung Institute of Technology, Bandung, Indonesia, ⁶South China Sea Marine Survey and Technology Center, State Oceanic Administration, Guangzhou, China, ⁷Agency for Marine and Fisheries Research and Human Resources, Ministry of Marine Affairs and Fisheries, Jakarta, Indonesia, ⁸Department of Marine Science, Faculty of Fisheries and Marine Science, Jenderal Soedirman University, Purwokerto, Indonesia, ⁹Ministry of Marine Affairs and Fisheries, Jakarta, Indonesia

Abstract Volume, heat and freshwater transports from the South China Sea (SCS) to the Java Sea through the Karimata Strait are estimated based on direct measurements of current, temperature, salinity, and satellite observations. Subject to strong seasonal variability, the volume, heat, freshwater transports are -1.98 ± 0.23 Sv (1 Sv = 10^6 m³/s), -209.68 ± 15.19 TW (1 TW = 10^{12} W), -99.87 ± 15.11 mSv (1 mSv = 10^{-3} Sv) in boreal winter, and 0.47 ± 0.20 Sv, 61.06 ± 15.46 TW, 31.67 ± 8.76 mSv in boreal summer, respectively (negative transport defined from SCS to Java Sea). The annual mean volume, heat and freshwater transports are -0.78 ± 0.12 Sv, -77.31 ± 4.99 TW, and -30.87 ± 6.15 mSv, respectively. The freshwater transport through Karimata Strait is as large as 42% of rainfall input to the entire Indonesian seas in boreal winter, thereby modulating the Indonesian Throughflow (ITF) through the “freshwater plug” effect in the Makassar Strait. The interannual variability of the transports is not significantly correlated to the Indian Ocean Dipole and El Niño-Southern Oscillation. There is a significant decreasing trend of volume and heat transports from the SCS to Java Sea over the period of 1997–2015, with a reduction of 0.26 Sv and 15 TW, respectively. The freshwater transport decreases 12.29 mSv by 2016 compared with that in 2009, equivalent to 33.2%–49.72% of the annual mean freshwater transport during 2009–2016. This decreasing trend would play contradictory roles in the decadal trend of ITF transport by building a “freshwater plug” in the southern Makassar Strait and a ‘buoyant plume’ in the Indo-Australian Basin, respectively.

Plain Language Summary Our previous studies revealed that the transport of heat and freshwater from the South China Sea (SCS) to the Java Sea by the Karimata Throughflow plays a role in balancing the heat and salt budgets in the SCS and modulating the Indonesian Throughflow (ITF) within the Makassar Strait. The early estimations were based on observations less than 1 year. In this study, ten-year records of direct measurements and satellite observations are used to calculate the volume, heat and freshwater transports of the Karimata Throughflow from 1993 to 2017. The updated climatological transports corroborate our previous estimation. The interannual variability of the Karimata Throughflow is not well correlated with either the Indian Ocean Dipole or El Niño-Southern Oscillation. The results also reveal significant decreasing trend of volume, heat and freshwater transports from the SCS to the Java Sea over the 1997–2015 period. The importance of the decreasing trends lies in the fact that it may modulate ITF by dual factors: first, the “freshwater plug” may be less effective in inhibiting water transport of the ITF in Makassar Strait; second, the “salinity effect” that suggests freshening of the buoyant plume in the Indo-Australian Basin favoring the enhancement of ITF would be depressed.

1. Introduction

The tropical Pacific and Indian Oceans are connected through the Indonesian seas and the South China Sea (SCS) (Figure 1a). The throughflow from the Pacific to the Indian Ocean, with two major branches, provides

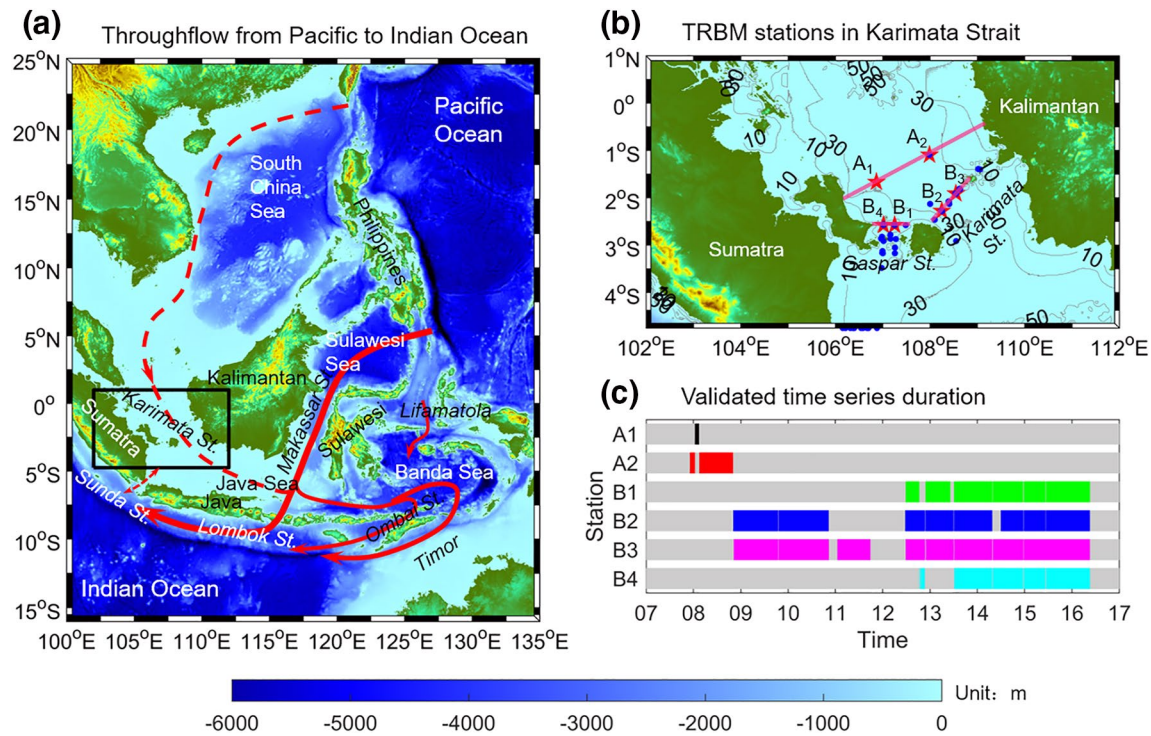


Figure 1. (a) Schematic map of the throughflow from the Pacific to Indian Ocean. The solid and dashed lines indicate the Indonesian Throughflow and the South China Sea branch, respectively. (b) Topography in the Karimata Strait (contours are water depths in meters) and the TRBM (red stars) and CTD (blue dots) stations of the SITE project. (c) Time series duration of the velocity profiles at each station. The color/gray band indicates time windows with/without data. CTD, Conductivity, Temperature, Pressure recorder; SITE, SCS-Indonesian Seas Transport/Exchange; TRBM, Trawl Resistant Bottom Mount.

the only interocean channel for water mass and heat transports at low latitudes (Figure 1a), enabling the so called “great ocean conveyor belt” closed (Broecker, 1991; Gordon & Fine, 1996; Talley, 2013). The branch through the eastern Indonesian seas is known as the Indonesian Throughflow (ITF), which transports volume over 10 Sv ($1 \text{ Sv} = 10^6 \text{ m}^3/\text{s}$) of water (Gordon et al., 2010, 2019; Liu et al., 2015; Sprintall et al., 2009, 2019; Susanto et al., 2012; Wijffels et al., 2008) and carries approximately 0.24–1.15 PW ($1 \text{ PW} = 10^{15} \text{ W}$) of heat from the Pacific to Indian Ocean (Hirst & Godfrey, 1993; Tillinger & Gordon, 2010; Vranes, 2002; Xie et al., 2019; Zhang et al., 2019). The other branch, through the SCS and the western Indonesian seas, is called the SCS branch or the SCS Throughflow (SCSTF) (Fang et al., 2003, 2005, 2009; Qu et al., 2006, 2009; D. X. Wang et al., 2006; Yu et al., 2007; Yaremchuk et al., 2009). The SCS branch connects the SCS and Java Sea through the Karimata and Gaspar Straits (Figure 1b). The Karimata Strait is located between the Belitung Island and Kalimantan Island with a width of 220 km and depth of 18–50 m. The Gaspar Strait is located between the Banka Island and Belitung Island with a width of 110 km and depths shallower than 40 m. For convenience, we collectively refer to the throughflow across the two straits as the Karimata Throughflow in the present study. The earliest estimation of water transport of the Karimata Throughflow was provided by Wyrki (1961) based on drifter bottles. The estimation suggests a volume transport of approximately 4.5 Sv from the SCS to the Java Sea in boreal winter, whereas 3 Sv from Java Sea to SCS in boreal summer. Compared to the well-recognized ITF, the contribution of the SCS branch to the interocean transport has been overlooked for decades because of its shallow water depth at the Karimata Strait. Nevertheless, later numerical studies suggest that the Karimata Strait transport plays important roles in the SCS heat/salt budget, with its annual mean heat and salt transports up to 0.35 PW and $1.1 \times 10^8 \text{ kg/s}$, respectively (Fang et al., 2003, 2009). Furthermore, the SCS branch (or SCSTF) is suggested to serve as a branch of the global ocean conveyor belt that connects the tropical Pacific and Indian oceans (Fang et al., 2005; Qu et al., 2005). The heat and freshwater transferred by this conveyor belt are estimated up to 0.2 PW and 0.1 Sv from the SCS into the Indonesian seas (Qu et al., 2006), making it nonnegligible not only in the heat and salt budget of the SCS (Fang et al., 2003; Zeng et al., 2009), but also in the modulation of ITF transport in the Makassar Strait (Gordon et al., 2012; Tozuka et al., 2007, 2009) and the El Niño-Southern Oscillation (ENSO) (Tozuka et al., 2015).

However, these numerical simulations show large uncertainty in Karimata Throughflow transport, with a wide range of annual mean volume transport from 0.3 to 4.4 Sv from the SCS to the Java Sea (Fang et al., 2003, 2005, 2009; Du & Qu, 2010; He et al., 2015; Lebedev & Yaremchuk, 2000; Liu et al., 2011; J. Wei et al., 2016; Yaremchuk et al., 2009). Therefore, a direct measurement of the velocity profile was urgently required, and it was then supported by the project “The SCS-Indonesian Seas Transport/Exchange (SITE) and Impact on Seasonal Fish Migration”, conducted jointly by researchers from China, Indonesia, and the United States since October 2006 (Susanto et al., 2010; Z. X. Wei et al., 2019). Based on the observation of the first two SITE cruises, the volume, heat and freshwater transports from the SCS to the Indonesian seas are estimated to be 3.6 Sv, 0.36 PW, and 0.14 Sv from 13 January to 12 February 2008, respectively (Fang et al., 2010). An updated estimation from SITE observations by defining negative values from the SCS to the Java Sea gives volume, heat and freshwater transports of -2.7 ± 1.1 Sv, -0.3 ± 0.11 PW, -0.18 ± 0.07 Sv in boreal winter, 1.2 ± 0.6 Sv, 0.14 ± 0.03 PW, 0.12 ± 0.04 Sv in boreal summer, and -0.5 ± 1.9 Sv, -0.05 ± 0.22 PW, -0.01 ± 0.15 Sv for the record from December 2007 to October 2008 (Susanto et al., 2013). Recently, Y. Wang et al. (2019) gives a climatological monthly mean estimation of the volume transport through the Karimata Strait by using SITE observations from November 2008 to June 2015. Their result estimates the volume transport of $-1.99/0.69$ Sv in boreal winter/summer, with an annual mean of -0.74 Sv.

Existing studies have well recognized the seasonal cycle of the Karimata Throughflow transport and its monsoon driven mechanism. Further investigations suggest that the Karimata Throughflow plays a two-fold role in the interocean volume transport, by reducing Makassar Strait transport through the “freshwater plug” effect (Fang et al., 2010; Gordon et al., 2012; Qu et al., 2005; Tozuka et al., 2007, 2009), and by contributing to the total volume transport, which are as large as 13% of the ITF transport (Fang et al., 2005; He et al., 2015; Xu & Malanotte-Rizzoli, 2013). However, in terms of interannual variability, there is no observed time series for Karimata Throughflow transport being published. Some of existing numerical simulations suggested the interannual variability is influenced by both ENSO and Indian Ocean Dipole (IOD) events (Du et al., 2010; He et al., 2015), but others argued no sensitivity in response to ENSO phase (Gordon et al., 2012).

The SITE project has carried out 19 cruises for the observation of water transport/exchange through the Karimata Strait from 2007 until 2016, thereby providing opportunity to reveal the interannual and long-term variations in the water transport of the Karimata Throughflow, as discussed in this study. The rest of the study is organized as follows. Section 2 describes the observation and data processing methods. Section 3 provides estimates of the volume, heat and freshwater transports of the Karimata Throughflow. Discussion and conclusions are given in Section 4, followed by a summary in Section 5.

2. Data and Methods

2.1. Data Description

The first two cruises of the SITE project were carried out in December 2007 and January 2008, during which there were two Trawl Resistant Bottom Mounts (TRBMs) deployed at A_1 and A_2 in the Karimata Strait (Figure 1b). The locations of the TRBM stations were changed from A_1 and A_2 to B_1 , B_4 , B_2 , and B_3 after 2008, with B_1 and B_4 in the Gaspar Strait between Bangka and Belitung, and B_2 , and B_3 in the Karimata Strait between Belitung and Kalimantan, respectively. The total water transport through the transects B_1B_4 and B_2B_3 is supposed to be equal to that through the transect A_1A_2 . There were four TRBMs, each of which launches an upward-looking, 300 or 600 kHz, self-contained Acoustic Doppler Current Profiler (ADCP), located at stations B_1 , B_4 , B_2 , and B_3 (Figure 1b). The bin size and sampling time interval were set to 2 m and 20 or 60 min for the ADCPs. The TRBMs were repeatedly deployed from November 1, 2008 through May 18, 2016.

Each of the TRBMs at stations B_1 , B_2 , and B_4 was equipped with an SEA-BIRD Scientific produced moored conductivity, temperature, pressure (CTD) recorder, i.e., the SBE37 CTD to measure bottom temperature, salinity and sea level elevation. The TRBM at station B_3 was equipped with an RBR Ltd. Temperature-pressure logger (TD). The sample intervals of the SBE37 CTD and RBR TD were set to 20 min. The CTD and TD were not equipped when deploying the TRBMs in some of the cruises, resulting in lack of measurements during the corresponding periods.

In addition to the bottom temperature and salinity records, satellite derived daily sea surface temperature (SST) and sea surface salinity (SSS) are also used in this study. The SST data are the National Oceanic and Atmospheric Administration (NOAA) High-resolution Blended Analysis of Daily SST and Ice products derived from the Advanced Very High Resolution Radiometer (AVHRR) data (Reynolds et al., 2007), and the Group for High Resolution Sea Surface Temperature (GHRSSST) (Donlon et al., 2007, 2009). The AVHRR SST is compiled on a $0.25^\circ \times 0.25^\circ$ grid covering the period from January 1981 to the present, and the GHRSSST is compiled on a $0.05^\circ \times 0.05^\circ$ grid covering the period from April 2006 to the present. Two SSS products are used in this study: the Soil Moisture Active Passive (SMAP) Level 3 SSS product with a horizontal resolution of $0.25^\circ \times 0.25^\circ$ from April 2, 2015, to November 28, 2017 (Fore et al., 2016), and the Soil Moisture and Ocean Salinity (SMOS) de-biased SSS L3 product version 3 mapped on a horizontal of $25 \times 25 \text{ km}^2$ from January 16, 2010 to December 25, 2017 (Boutin et al., 2016, 2018; Kolodziejczyk et al., 2016).

The sea surface height (SSH) data are the Version 5.0 of daily gridded absolute dynamic topography products produced by the Segment Sol Multimissions d'Altimétrie d'Orbitographie et de Localisation Précise/Data Unification and Altimeter Combination System (SSALTO/DUACS) and distributed by the Archiving, Validation, and Interpretation of Satellite Oceanographic (AVISO), with support from Centre National d'Etudes Spatiales (CNES) (<http://www.aviso.altimetry.fr/duacs/>). The dataset is daily, at a resolution of $0.25^\circ \times 0.25^\circ$, which is available from October 1992 to the present (Ducet et al., 2000). The sea surface wind (SSW) data are from the Cross Calibrated Multi-Platform (CCMP) Version 2.0 with a horizontal resolution of $0.25^\circ \times 0.25^\circ$ and time interval of 6 h, provided by the National Aeronautics and Space Administration (NASA) since 2009 (Atlas et al., 2011). The wind data used for calculating the cross-equatorial flow index and the East Asia winter monsoon index are the ERA5 global reanalysis dataset provided by the European Centre for Medium-Range Weather Forecasts (ECMWF). The data resolution is $0.25^\circ \times 0.25^\circ$ (Hersbach et al., 2020). The bathymetry adopted for the transport estimation is ETOPO1, obtained from <http://www.ngdc.noaa.gov/mgg/global>, which has a horizontal resolution of $1^\circ/60 \times 1^\circ/60$.

2.2. Methods

The quick quality controlled records of velocity for each TRBM are linearly interpolated onto a 2-m-depth grid for each hour time step. The missing velocities in the surface layer (upper 2–6 m due to surface reflection contamination of the ADCP) are replaced by extrapolation that assumes the vertical shear of velocities is constant to the surface (Fang et al., 2010; Sprintall et al., 2009; Susanto et al., 2012). After tidal removal by a 25-h low-pass filter, the vertically gridded velocity time series is then daily averaged and projected to the normal direction of the sections across the straits (along-strait velocity, hereafter ASV) in order to calculate the transport. The normal directions in Gaspar Strait (section B14) and Karimata Strait (section B23) are 0° and 309° referenced to true north, respectively. The time series of ASV profiles at each station have missing values during the SITE period (Figure 1c), which are reconstructed by a regressed model based on the SSH gradient and local SSW along the strait (Wang et al., 2019).

Assuming that the variation in the ASV is mainly caused by the variation in local winds and sea surface slope, and thus it can be empirically expressed as:

$$ASV = ASV_0 + a_1 \times U_{\text{wnd}} + a_2 \times V_{\text{wnd}} + a_3 \times \Delta ADT + \varepsilon \quad (1)$$

where ASV_0 is the intercept value and indicate the ASV without local winds and sea surface slope; a_1 , a_2 , and a_3 are the regression coefficients; U_{wnd} and V_{wnd} are the zonal and meridional components of local wind, respectively; ΔADT is the difference of area averaged SSH between the south ($4.375\text{--}5.625^\circ\text{S}$, $106.125\text{--}108.625^\circ\text{E}$) and north ($0.625^\circ\text{S}\text{--}0.625^\circ\text{N}$, $106.125\text{--}108.625^\circ\text{E}$) of the Gaspar and Karimata straits; and ε is the residual term. The correlation coefficients between the observed and regressed ASVs at all of the four stations are greater than 0.82, which is above the 99% confidence level. The mean absolute error for the proxy is approximately 6 cm/s.

The time series of temperature and salinity profiles are derived from sea bottom temperature and salinity measured by the TRBMs as well as the SST and SSS, respectively. For simplicity, we assume that the

vertical shear of temperature and salinity in the boreal spring to winter seasons are independent of time. In this study, seasons refer to the Northern Hemisphere, that is, spring for March to May, summer for June to August, fall for September to November, and winter for December to February of the next year. Taking the values of winter as an example, the vertical shear is as follows:

$$\frac{dT}{dz} \Big|_{\text{winter}} = \frac{T_{i+1}^0 - T_i^0}{\Delta z} \quad (2)$$

where T_i is the water temperature at the i th depth, Δz is the vertical interval. For daily SST time series in December, January, and February, the projected temperature at each depth is calculated as follows:

$$T_{i+1} = T_i + T_{i+1}^0 - T_i^0, T_1 = \text{SST} \quad (3)$$

To estimate the transport through each strait, the TRBM station observations were laterally interpolated between the stations and extrapolated to the strait sidewalls along the sections B14 and B23 based on the ETOPO1 topography. The interpolation/extrapolation scheme used in this study is the logarithmic-profile-cubic-spline interpolation with no slip condition at sidewalls (Fang et al., 2010; Y. Wang et al., 2019).

The water volume transport F_V through a strait is calculated by the integration of the normal velocity in the section:

$$F_V = \sum_{k=1}^{k=n} \left[\Delta z_k \sum_{i=1}^{i=m} \Delta l_i v_{i,k} \right] \quad (4)$$

where i and k indicate serial numbers of each horizontal and vertical grid box in the section, respectively. The $v_{i,k}$ is the averaged normal velocity across the section within the grid box of Δl_i by Δz_k in width and thickness. Negative values (southward transport) indicate volume transport from the SCS to the Java Sea.

The heat transport F_H is calculated as follows:

$$F_H = C_p \sum_{k=1}^{k=n} \left[\Delta z_k \sum_{i=1}^{i=m} \Delta l_i \rho_{i,k} (T_{i,k} - T_0) v_{i,k} \right] \quad (5)$$

where $T_{i,k}$ and $\rho_{i,k}$ are the averaged temperature and density in the grid box, respectively. T_0 is the reference temperature, which is 3.72°C, as suggested by Fang et al. (2010). The specific heat ratio C_p is set to $3.89 \times 10^3 \text{ J kg}^{-1} \text{ }^\circ\text{C}^{-1}$. Negative values indicate heat transport from the SCS to the Java Sea.

The salt transport is calculated by

$$F_S = \sum_{k=1}^{k=n} \left[\Delta z_k \sum_{i=1}^{i=m} \Delta l_i S_{i,k} v_{i,k} \right] \quad (6)$$

where $S_{i,k}$ is the averaged salinity within the grid box.

The freshwater transport is calculated from

$$F_w = \sum_{k=1}^{k=n} \left[\Delta z_k \sum_{i=1}^{i=m} \Delta l_i \left(\frac{S_0 - S_{i,k}}{S_0} \right) v_{i,k} \right] \quad (7)$$

where S_0 is a reference salinity, which equal to the mean salinity of the SCS, taken as 34.62 following Fang et al. (2010). Negative values indicate freshwater transport from the SCS to the Java Sea.

The Empirical Mode Decomposition (EMD) methods are used as time filters to extract the interannual signal of time series by adding the Intrinsic Mode Functions (IMFs) with cycles between 2 and 9 years together (Huang et al., 1998). The Morlet wavelet is adopted as the mother wavelet in the wavelet analysis. The 95% confidence level for the wavelet analysis is calculated based on a red noise background spectrum with an autoregressive lag-1 correlation of 0.72 (Torrence & Compo, 1998).

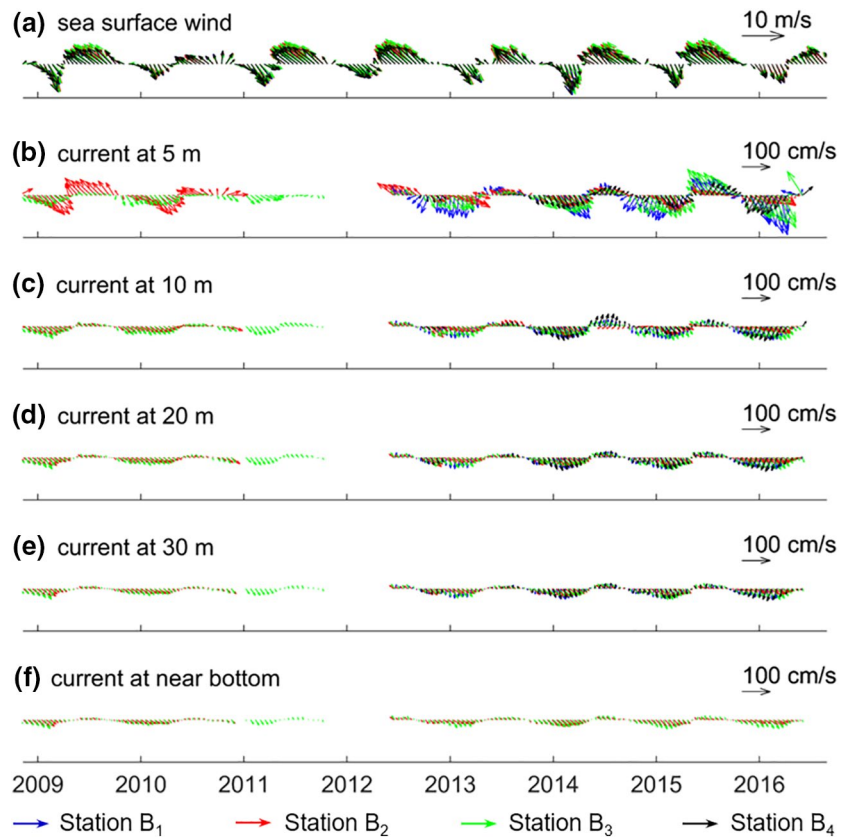


Figure 2. Time series of (a) monthly sea surface wind and (b)–(f) flow vectors at 5, 10, 20, 30, and near bottom in the Gaspar and Karimata straits, respectively. The blue, red, green, and black vectors are in station B₁, B₂, B₃, and B₄, respectively. Upward vectors refer to true north.

Since the time coverage of the datasets is inconsistent, we describe the interannual anomalies by removing the monthly mean climatology with respect to the base period from 2000 to 2014, while most of the datasets are covered and the extreme El Niño event of 2015–2016 is excluded. The Oceanic Niño Index (ONI) is provided by NOAA (<https://ggweather.com/enso/oni.htm>). The Dipole Mode Index (DMI) for the IOD is defined as the differences of area averaged SST anomalies between the western (10°S–10°N, 50°E–70°E) and southeastern (10°S–0°, 90°E–110°E) tropical Indian Ocean (Saji et al., 1999). The maritime continent cross-equatorial flow index is defined as the area averaged meridional wind at 925 hPa within (5°S–5°N, 102.5°E–110°E) (Zhao & Lu, 2020). The East Asia winter monsoon index is defined as the area averaged meridional wind at 1,000 hPa within (10°N–30°N, 115°E–130°E) in winter (Ji & Sun, 1997).

3. Results

3.1. Flow Velocity, Temperature and Salinity

The widths of the sections at the Gaspar and Karimata straits are 90 and 120 km, with maximum depths of 34 and 40 m, respectively, according to the bathymetry of the ETOPO1 dataset. The time series of wind and flow vectors at Stations B₁ and B₄ in the Gaspar Strait, B₂ and B₃ in the Karimata Strait, are shown in Figure 2. The flow in the two shallow straits is dominantly forced by monsoon. The flow shows similar directions at different depths, with daily mean velocities up to 150 cm/s at the surface and decreasing to approximately 20 cm/s at the bottom. The currents in the Gaspar and Karimata straits basically show barotropic-dominated signatures and are attenuated by the strong bottom friction (Y. Wang et al., 2019). In addition, there are still southward/northward flow while the northwesterly/southeasterly winds diminish, implying that the sea surface slope is another driving force of the throughflow in the Gaspar and Karimata straits.

The along-strait momentum equation can be written as follows:

$$\frac{\partial \tilde{u}}{\partial t} - f\bar{v} = -g \frac{\partial \eta}{\partial x} + \frac{\tau_{sx} - \tau_{bx}}{\rho H} \quad (8)$$

where \tilde{u} and \bar{v} are the vertical mean current velocities of the along- and across-strait components, respectively; η is the SSH; f , g , ρ , and H are the Coriolis parameter, gravitational acceleration, mean water density, and mean water depth, respectively; and τ_{sx} and τ_{bx} are the along strait components of wind stress and bottom frictional stress, respectively, which are related to the sea surface wind and near bottom currents as follows:

$$\tau_{sx} = C_{ds} \rho_a |V_a| u_a \quad (9)$$

$$\tau_{bx} = C_{db} \rho |V_b| u_b \quad (10)$$

where C_{ds} and C_{db} are drag coefficients of wind stress and bottom frictional stress, assumed constants with value of $\sim 2 \times 10^{-3}$; ρ_a is the air density, taken to be 1.169 kg/m^3 for a mean sea level air pressure of $1.01 \times 10^5 \text{ Pa}$ and a mean air temperature of 28°C ; $|V_a|$ and $|V_b|$ are the sea surface wind and near bottom current speed; and u_a and u_b are the along-strait components of the sea surface wind and the near bottom current, respectively.

According to the observations, the magnitude of $\partial \tilde{u} / \partial t$ is on the order of $\sim 5 \times 10^{-8} \text{ m/s}^2$, the Coriolis term can be ignored near the equator, the SSH gradient forcing is on the order of $\sim 3.5 \times 10^{-6} \text{ m/s}^2$, and the surface and bottom stresses are roughly on the order of $\sim 2.5 \times 10^{-6} \text{ m/s}^2$. Therefore, the dominant dynamic balance is established by the SSH gradient forcing, the wind stress and the bottom friction.

This dynamic balance is well represented by the fact that the variation in vertically averaged ASV at all four stations coincides with the area-averaged SSH difference between the south ($4.375\text{--}5.625^\circ\text{S}$, $106.125\text{--}108.625^\circ\text{E}$) and north ($0.625^\circ\text{S}\text{--}0.625^\circ\text{N}$, $106.125\text{--}108.625^\circ\text{E}$) of the Gaspar and Karimata straits (Figure 3a). The correlation coefficients between the daily SSH gradient and ASV at the four stations are 0.897, 0.870, 0.863, and 0.899, respectively, which are above the 95% confidence level. The daily local SSW are also significantly correlated with the ASV at the four stations, with mean correlation coefficients of $-0.785/0.825$ for zonal/meridional winds. These high correlations encourage us to extend the observed ASV to a much longer time series based on the satellite observed SSH and SSW data. By using a regression method (Y. Wang et al., 2019), we reconstruct the daily ASV time series from 1993 to 2017, which are used for the analysis of the water transport variations in the Gaspar and Karimata straits.

Figure 3b shows the bottom temperature measured by the TRMBs and SST derived from satellites. The bottom temperature and SST at the four stations are synchronous with each other, showing double peaks during one calendar year. The maximum temperatures ($\sim 30.2^\circ\text{C}$) occur in May and the second peak ($\sim 29.5^\circ\text{C}$) occurs in November during most of the observation period. The minimum temperatures ($\sim 28.2^\circ\text{C}$) occur in February. During the SITE period, the bottom temperature is $0.18 \pm 0.74^\circ\text{C}$ and $0.06 \pm 0.71^\circ\text{C}$ lower than the AVHRR and GHRSSST, respectively. The GHRSSST is generally $0.07 \pm 0.27^\circ\text{C}$ smaller than the AVHRR. On the other hand, the temperature profiles measured by CTD show that the mean difference of sea surface and bottom temperature is 0.09°C in December, 0.18°C in April and May, 0.05°C in June and August, and 0.72°C in September and November (Figure 4). The vertical structures of the temperature show a near-linearly decreasing trend instead of a shallow mixed layer at most of the stations except in April-May. Nevertheless, the station averaged temperature profile in April-May also represents a near-linearly decreasing trend with depth, suggesting that for variations with seasonal or longer time scales, the temperature profile can be derived from SST based on the simple assumption given in Section 2.2. The average temperature and salinity profiles derived from the satellite SST and SSS basically show similar vertical structures in comparison with the CTD measurements, albeit with a systematic shift (Figure 4). We also notice that there are different vertical structures for single CTD profiles (which also rely on weather conditions such as rainfall); therefore, it is not accurate when estimates the daily profiles based on satellite observations. However, for time scales longer than seasonal cycle, it could provide a good reference. Unfortunately, since the CTD profiles are too few, it is also difficult to give an error estimation; instead, we have tried to use three datasets of temperature/

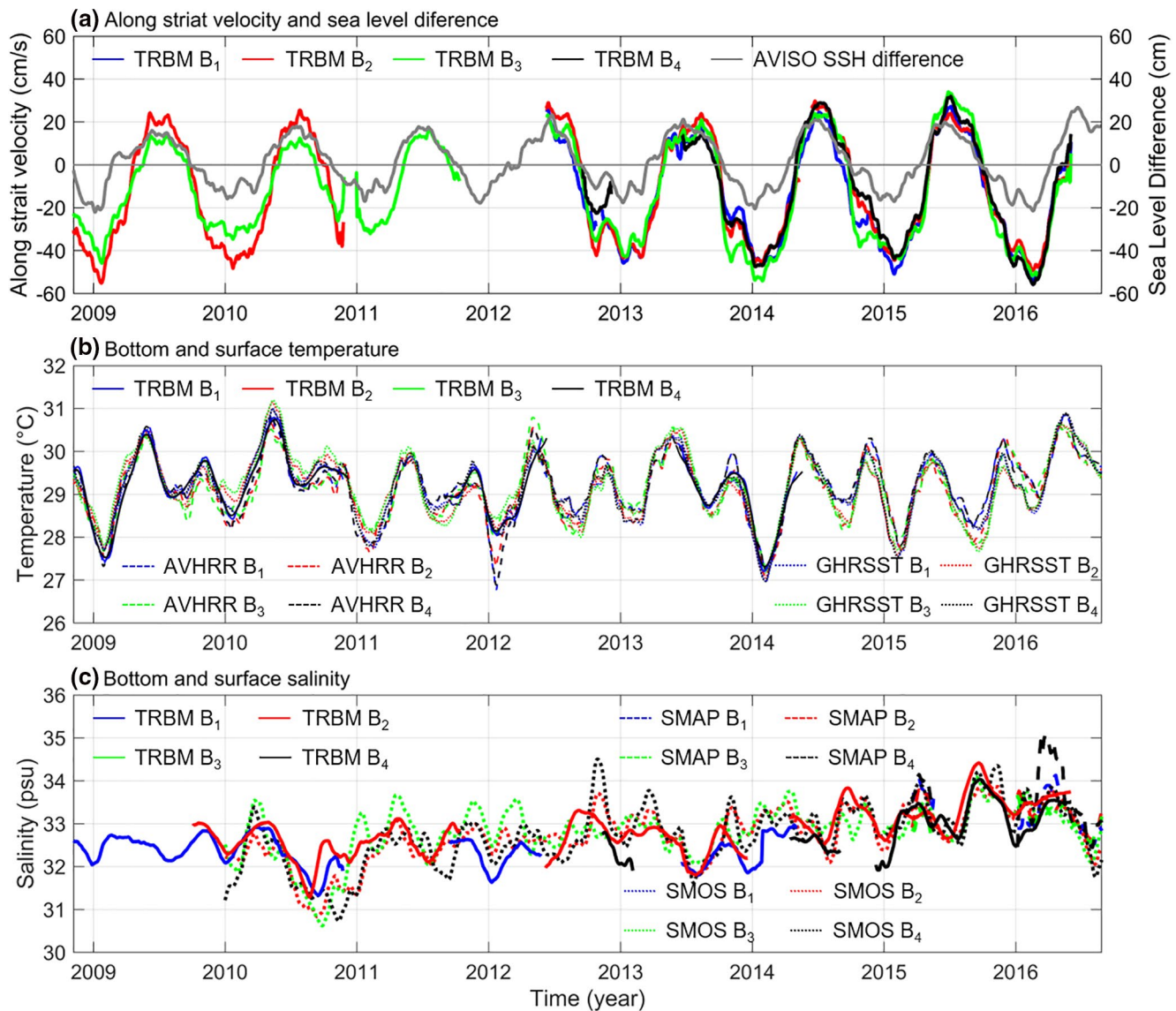


Figure 3. (a) Vertically averaged along strait velocity (positive northward) and SSH difference between the south (4.375–5.625°S, 106.125–108.625°E) and north (0.625°S–0.625°N, 106.125–108.625°E) of the Gaspar and Karimata straits. (b) Bottom temperature measured by CTD on board of TRBMs (solid lines) and sea surface temperature from AVHRR (dashed lines) and GHRSSST (dotted lines). (c) Bottom salinity measured by CTD on board of TRBMs (solid lines) and sea surface salinity from SMAP (dashed lines) and SMOS (dotted lines). AVHRR, Advanced Very High Resolution Radiometer; CTD, Conductivity, Temperature, Pressure recorder; GHRSSST, Group for High Resolution Sea Surface Temperature; SMAP, Soil Moisture Active Passive; SMOS, Soil Moisture and Ocean Salinity; TRBM, Trawl Resistant Bottom Mount.

salinity time series, including two satellite products and one in situ measurement, to estimate the heat and freshwater transports.

Figure 3c shows the bottom salinity measured by the TRMBs and SSS derived from satellites. The bottom salinity shows similar annual cycle in comparison with temperature, but with double peaks in April (32.99 psu) and October (33.06 psu). The satellite SSS products do not coincide with the bottom salinity from TRBMs at the daily time scale as those of SST and bottom temperature. However, it is consistent with the double peaks for the SSS annual cycle. Moreover, both satellite and TRBM reveal an increasing salinity trend approximately 0.13 psu/year in the Gaspar and Karimata straits since October 2008. This salinity trend has accelerated up to approximately 0.28 psu/year since January 2012. Previous investigations suggest dual roles of Karimata Strait transport in the total ITF volume transport: by contributing to the total transport on the one hand, and by reducing the Makassar Strait transport on the other hand. Therefore, the salin-

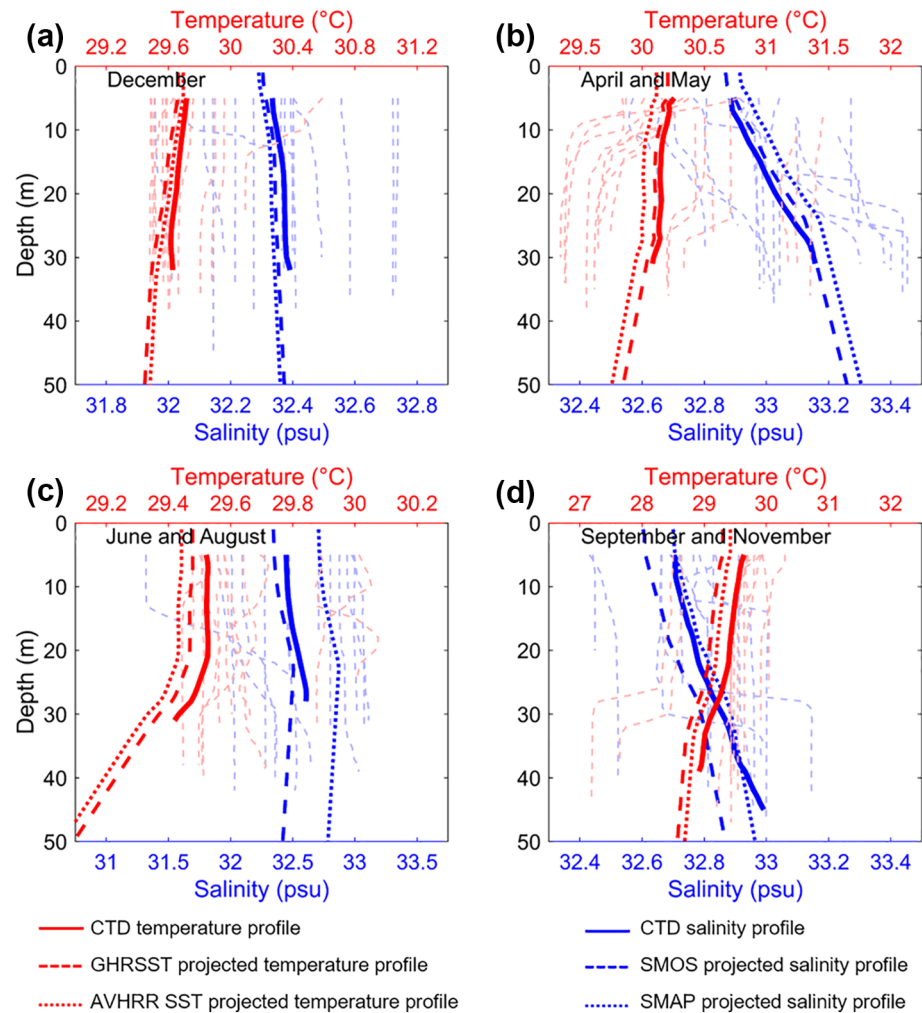


Figure 4. Temperature and salinity profiles from the CTD casts and reconstructed from satellite SST and SSS in (a) December, (b) April and May, (c) June and August, and (d) September and November. Light dashed red and blue lines are temperature and salinity profiles from single CTD cast. Solid dark red and blue lines are temperature and salinity profiles averaged from the CTD casts. Dark dashed and dotted red lines are averaged temperature profiles derived from GHRSSST and AVHRR SST data. Dark dashed and dotted blue lines are averaged salinity profiles derived from SMOS and SMAP SSS data. AVHRR, Advanced Very High Resolution Radiometer; CTD, Conductivity, Temperature, Pressure recorder; GHRSSST, Group for High Resolution Sea Surface Temperature; SMAP, Soil Moisture Active Passive; SMOS, Soil Moisture and Ocean Salinity.

ity trend in the Gaspar and Karimata straits may influence the interactions between the SCS branch and the ITF as less fresh water is transported to the Java Sea. Similar to those of temperature, the station-averaged salinity profile also represents a linear decreasing trend with depth (Figure 4), suggesting that for variations with seasonal or longer time scales, the salinity profile can be derived from the SSS and/or bottom salinity based on the simple assumption in Section 2.2.

3.2. Volume Transport

Figure 5 shows the seasonal variability in the net volume transport from the SCS to the Java Sea across the transects A and B, respectively. A previous estimation of the volume transport across transect A suggested -3.6 ± 0.8 Sv from 13 January to 12 February 2008 (Fang et al., 2010). Susanto et al. (2013) estimated the averaged volume transport across transect A was -2.7 ± 1.1 Sv from December 2007 to March 2008, and 1.2 ± 0.6 Sv from May to September 2008. Of the averaged volume transport during the entire obser-

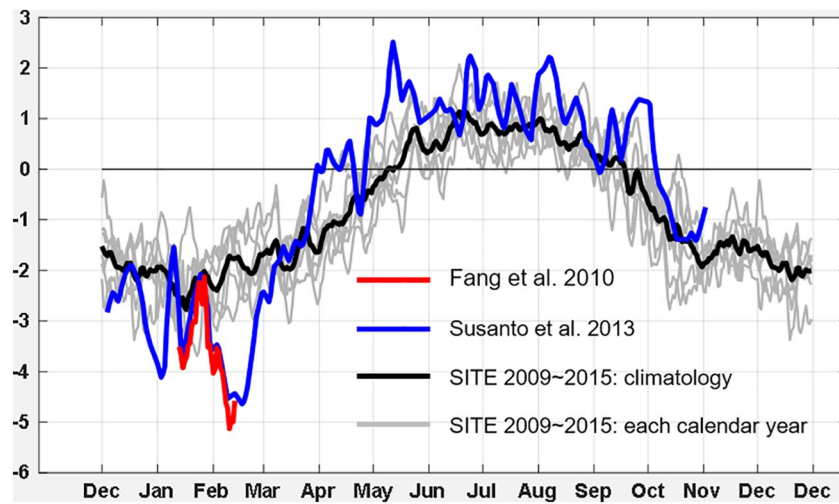


Figure 5. Total volume transport through transect A estimated by Fang et al. (2010) from January 13 to February 12, 2008 (red line) and Susanto et al. (2013) from December 4, 2007 to November 1, 2008 (blue line); and through the transect B from November 7, 2008 to May 18, 2016 (gray and black lines represent each calendar year and the climatological result, respectively). Negative values indicate southward transport from the SCS to the Java Sea. SCS, South China Sea.

vation period (from 4 December 2007 to 1 November 2008), Susanto et al. (2013) gave an estimation of -0.5 ± 1.9 Sv. In comparison, the climatological total volume transports over the period of 2009–2016 across the transects of B14 plus B23 give values of -1.98 ± 0.23 Sv from December to March, 0.47 ± 0.20 from May to September, and 0.78 ± 0.12 Sv in annual mean.

By applying a regression model, we calculate the ASV at stations B_1 to B_4 from 1993 to 2017 based on AVISO SSH and CCMP SSW data. The vertically averaged ASV at each station shows that the predicted and measured velocities match well with each other (Figures 6a–6d). The vertically averaged ASV also shows dominant seasonal variability forcing by monsoon, with annual mean velocities of -16 and -14 cm/s in the Gaspar and Karimata straits, respectively. The vertical distributions of ASV interannual anomalies in Gaspar and Karimata straits are shown in Figure 6e and 6f, respectively. The interannual variability of ASV profiles in the Gaspar and Karimata straits are generally synchronized with each other (Figures 6e–6f). The maximum anomalies reach approximately 9 and 6 cm/s in the Gaspar and Karimata straits, respectively, which occur near the surface layer shallower than 10 m. The periods of strong throughflow (negative anomalies) are identified as 1994–1995, 1999–2000, 2001–2002, 2004, 2007, and 2013–2014. The periods of weak throughflow (positive anomalies) are identified during 1996–1997, 1998–1999, 2008–2009, 2011–2012, and 2016–2017. In addition to the interannual variability, a significant positive trend is also found in Figure 6e and 6f, implying a slowdown of southward flow in both the Gaspar and Karimata straits since 2008. This may have resulted in a decreasing water transport from the SCS to the Java Sea since 2008.

Figure 7 shows the total volume transport anomalies and the IMFs and residual decomposed from the total volume transport. The IMF1 represents the seasonal variation in transport, showing positive/negative values during the southeast/northwest monsoon seasons. The seasonal variation is the dominant mode, whose amplitude could reach 1.5 Sv (Figure 7b). The IMF2 and IMF3 with periods of 2.5 and 4.5 years represent the interannual variations (Figure 7c and 7d). The sum of IMF2 and IMF3 is shown in Figure 7a in order to compare with the interannual anomalies of the total volume transport. The transport anomalies are consistent with the sum of IMF2 and IMF3 except for an additional ascending trend, which is caught by the residual of the EMD analysis. The amplitude of interannual variability is approximately 0.10 ± 0.05 Sv with the maximum amplitude up to 0.22 Sv. The period of IMF4 is 14.2 years, suggesting a decadal variation in volume transport (Figure 7e). The positive periods of decadal variability are 1993–2003 and 2010–2015, whereas the negative periods are 2003–2009 and 2016 to the present. The residual of the EMD analysis shows ascending trend of 0.02 Sv per year over the period of 1997–2014, implying that volume transport toward the Java Sea has decreased by as much as 0.26 Sv after 2014 in comparison with that before 1997.

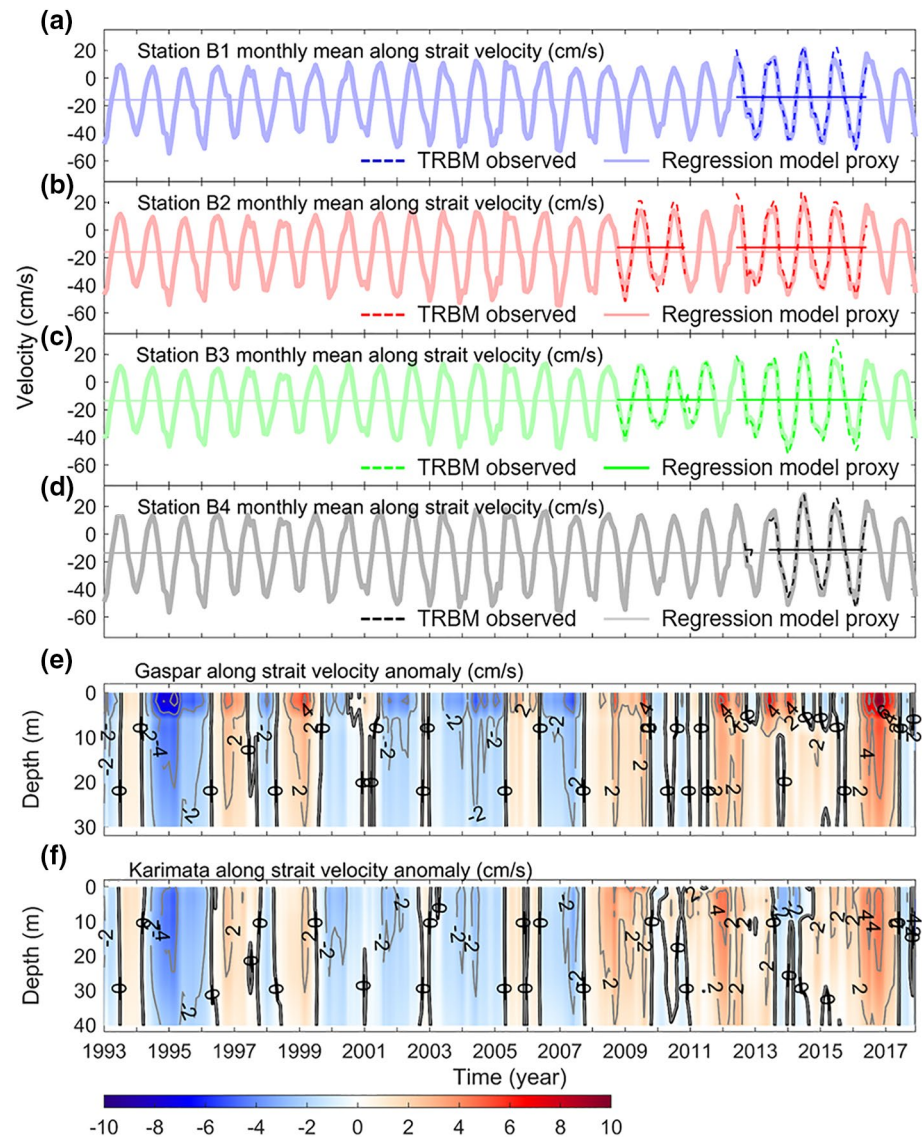


Figure 6. Monthly mean along-strait velocity at Stations (a) B₁, (b) B₂, (c) B₃, (d) B₄, and vertical distribution of along-strait velocity anomaly time series in (e) Gaspar and (f) Karimata straits. The horizontal lines in (a)–(d) represent the mean velocity. The light and dark lines in (a)–(d) indicate the regressed and observed velocities, respectively. Negative values indicate southward flow from the South China Sea to the Java Sea. The time series in (a)–(f) are smoothed with 13-month running mean to filter high-frequency noise.

The wavelet analysis of the filtered interannual volume transport (IMF2+IMF3) is shown in Figure 8a. The results show significant interannual signals with typical periods of 1.8–3.1 and 2.6–3.8 years during 1993–2001 and 2004–2014, respectively. The Hilbert spectral energy of the sum of IMF2 and IMF3 shows energy larger than the mean energy plus half of its standard deviation during 1993–1996, 2006–2007, 2009, and 2016. Together with the time series of IMF2+IMF3 (solid line in Figure 7a), the strong interannual transport events (i.e., more volume transport from the SCS to Java Sea) are identified during 1995, 2007, and 2013; and the weak interannual transport events are identified during 1993–1994, 2005–2006, 2009–2010, and 2016–2017. The strong and weak events generally peak in boreal summer and winter, respectively. Of particular interest is that the interannual events of volume transport are not statistically correlated with either ENSO or IOD events, since they could occur during either normal or IOD/ENSO years, but not occur during the strong IOD/ENSO event of 1997–1998. The correlations between the interannual volume transport and the DMI and ONI indices are -0.17 and 0.18 , respectively, which are both below the 95% confidence level.

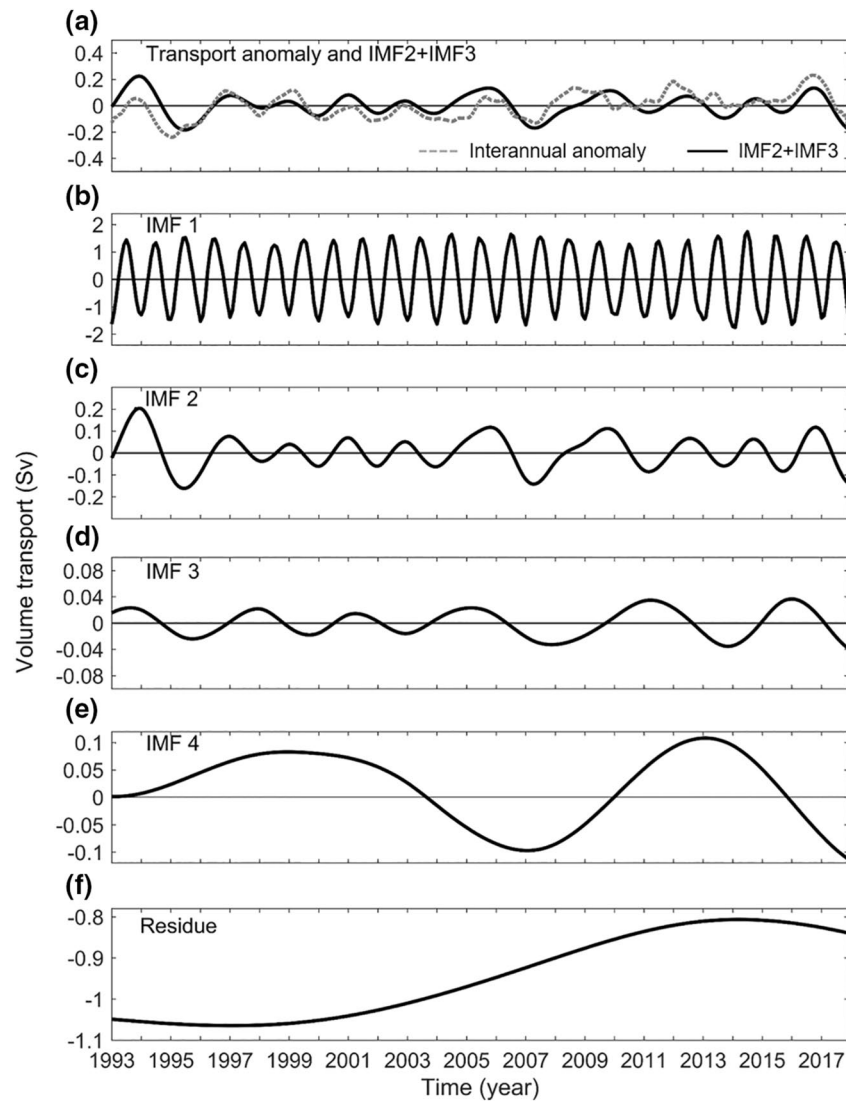


Figure 7. (a) Total volume transport anomalies with a running mean window of 13 months (dashed line) and IMF2+IMF3 (solid line); (b)–(e) The IMFs of EMD analysis of the total volume transport through the Gaspar and Karimata straits. (f) The residual of the EMD analysis. EMD, Empirical Mode Decomposition; IMF, Intrinsic Mode Function.

3.3. Heat and Freshwater Transports

The Karimata Throughflow carries an annual mean heat flux of approximately 77.31 ± 4.99 TW ($1 \text{ TW} = 10^{-3}$ PW) from the SCS to the Java Sea (Table 1). In winter, the heat transport is 209.68 ± 15.19 TW from the SCS to the Java Sea, whereas 61.06 ± 15.46 TW from the Java Sea to the SCS in summer (Table 1). Meanwhile, the freshwater transport of the Karimata Throughflow gives an estimation of annual mean value at -30.87 ± 6.15 mSv ($1 \text{ mSv} = 10^{-3}$ Sv) (Table 2). The seasonal cycle of freshwater transport coincides with those of the volume and heat transport, which suggests a seasonal mean transport of -99.87 ± 15.11 and 31.67 ± 8.76 mSv in boreal winter and summer, respectively (Table 2). Different investigations show a wide range of annual mean estimates of ITF heat transport from 0.39 to 1.15 PW, with an averaged value of 0.66 PW (Hirst & Godfrey, 1993; Tillinger & Gordon, 2010; Vranes, 2002; Xie et al., 2019; Zhang et al., 2019). Therefore, the contribution of annual mean heat transport carried by the Karimata Throughflow could be as large as $\sim 15\%$ of that carried by the ITF, although the annual mean volume transport of the Karimata Throughflow is only 5% of the ITF. This contribution becomes more important and, roughly equals more

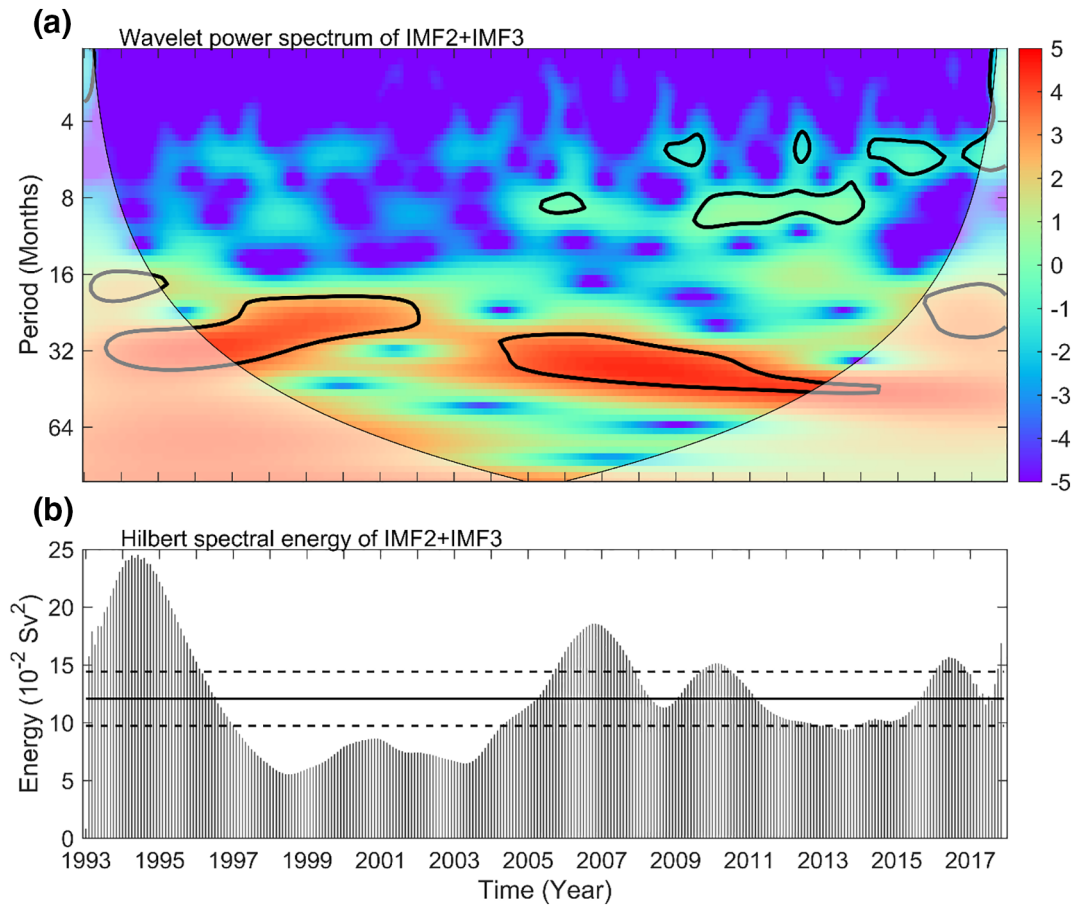


Figure 8. (a) Wavelet power spectrum and (b) Hilbert spectral energy of the interannual volume transport anomalies (IMF2+IMF3). The areas enclosed by the black contours in (a) are above the 95% significance level. The black solid and dashed lines in (b) indicate the mean Hilbert spectrum energy and the 0.5 standard deviation above and below the mean value. IMF, Intrinsic Mode Function.

than half of the ITF heat transport in boreal winter, while the heat transport of the Karimata Throughflow reaches its peak of approximately 0.21 PW, but is expected to be at a value smaller than its mean state for the ITF (Gruenburg & Gordon, 2018; Vranes, 2002).

The anomaly as well as the IMFs and residual derived from the Karimata Throughflow heat transport are shown in Figure 9. The heat transport anomalies derived from CTD measurements and satellite SST are in good agreement with each other (Figure 9a). The interannual heat transport is comprised of IMF2 and IMF3 of the EMD analysis, with periods of 2.5 and 4.5 years, respectively. The amplitude of interannual variability is approximately 8.54 ± 4.90 TW with the maximum amplitudes up to 17.11 TW. The Karimata Throughflow heat transport is primarily dominated by seasonal variability driven by monsoon, with seasonal amplitude up to 131.94 ± 12.54 TW, which is about 10 times the values for interannual and decadal

Table 1
Climatological Heat Transport Through the Gaspar and Karimata Straits (Unit: TW)

	Jan	Feb	Mar	Apr	May	Jun	Jul	Aug	Sep	Oct	Nov	Dec	Annual mean
CTD	-235.86	-202.84	-181.39	-91.14	11.49	78.76	87.47	62.27	-11.43	-131.78	-170.89	-208.42	-82.81
AVHRR	-223.50	-197.56	-146.45	-58.99	17.06	54.45	62.92	39.19	-11.87	-92.97	-147.00	-207.50	-76.02
GHRSSST	-223.33	-187.16	-144.72	-61.03	10.24	55.19	65.95	43.31	-6.58	-87.18	-140.80	-200.96	-73.09

Abbreviations: AVHRR, Advanced Very High Resolution Radiometer; GHRSSST, Group for High Resolution Sea Surface Temperature.

Table 2
Climatological Freshwater Transport Through the Gaspar and Karimata Straits (Unit: mSv; 1 mSv = 10⁻³ Sv)

	Jan	Feb	Mar	Apr	May	Jun	Jul	Aug	Sep	Oct	Nov	Dec	Annual mean
CTD	-124.14	-89.96	-74.66	-32.55	5.04	36.22	44.28	29.08	-3.42	-45.48	-69.56	-107.83	-36.08
SMOS	-113.10	-84.85	-63.56	-30.47	4.51	32.31	44.08	31.57	-5.68	-47.19	-62.12	-94.85	-32.45
SMAP	-112.89	-79.48	-37.68	-19.47	9.85	25.02	23.65	18.83	-0.48	-21.46	-46.18	-91.77	-27.67

Abbreviations: SMAP, Soil Moisture Active Passive; SMOS, Soil Moisture and Ocean Salinity.

variations (Figures 9b–9e). The IMF4 shows decadal variability with a period of 14.2 years, which is consistent with that of volume transport (Figure 9e). In addition to these periodic variations, the Karimata Throughflow heat transport also shows a significant ascending trend of 0.78 TW per year over the period of 1998–2015, suggesting reduction of heat transport from the SCS to the Java Sea by around 15 TW over the past two decades. This decreasing trend of southward heatflux is closely related to the decadal change of upper ocean heat content in the SCS associated with the Interdecadal Pacific Oscillation (IPO) (Xiao et al., 2019, 2020).

Considering that the current and temperature in the Gaspar and Karimata straits can be decomposed into seasonal cycles and anomalies $V = \bar{V} + V'$, and $T = \bar{T} + T'$, then the heat transport can be written as follows:

$$F_H = C_p \rho_0 \iint \left[(\bar{T} - T_0) \bar{V} + (\bar{T} - T_0) V' + \bar{V} T' + T' V' \right] dx dz \quad (11)$$

where the first through third terms of the right-hand side represent the contributions from climatological state, velocity and temperature variations, respectively. The fourth term has relatively smaller values and thus can be ignored. The sea water density is set to a constant of 1,024 kg/m³ for simplicity. The values of these four terms are plotted in Figure 10. The results show that both the velocity and temperature anomalies contribute to the interannual variation in the Karimata Throughflow heat transport, accounting for approximately 6.14 and 0.94 TW, respectively (Figure 10b and 10c). The velocity anomalies also explain a decreasing trend of southward heat transport of the Karimata Throughflow by 0.86 TW per year during the period of 1993–2017. In contrast, the temperature anomalies induce an increasing trend of 0.09 TW per year in the southward heat transport, which may be associated with basin scale warming in the SCS.

By the combination of direct measurement of near bottom salinity and satellite remote sensing of SSS, the freshwater transport time series could be extended from October 2008 to December 2017 (Figure 11). The freshwater transport anomaly is in phase with the sum of IMF2 and IMF3 (Figure 10a), which suggests typical interannual periods of 2.5–4.5 years (Figure 11c and 11d). Seasonal variability, of which the amplitude reaches 66.06 ± 7.06 mSv, is the largest contribution to the freshwater transport variations (Figure 11b). In comparison, the amplitude of interannual freshwater transport is only 3.42 ± 3.58 mSv. The largest interannual freshwater anomalies occurred in 2011 and 2012, showing an increase and decrease in freshwater transport from the SCS to the Java Sea by 6.55 and 7.00 mSv, respectively (Figure 11a). The residual of the EMD analysis shows an ascending trend of 1.54 mSv per year over the period of 2009–2016 (Figure 11e). In other words, the freshwater transport from the SCS to the Java Sea has reduced by approximately 12.29 mSv in 2016 compared with 2009. This reduction is equal to around 33.2%–49.72% of the annual mean freshwater transport from 2009 to 2016.

Similarly, the freshwater transport of the Karimata Throughflow can be given by

$$\iint \left[\frac{(S_0 - S) \bar{V}}{S_0} + \frac{(S_0 - S) V'}{S_0} - \frac{S' \bar{V}}{S_0} - \frac{S' V'}{S_0} \right] dx dz$$

where the first to third terms of the right-hand side represent the contributions from climatological state, velocity and salinity variations, respectively. The fourth term is the higher-order term. The values

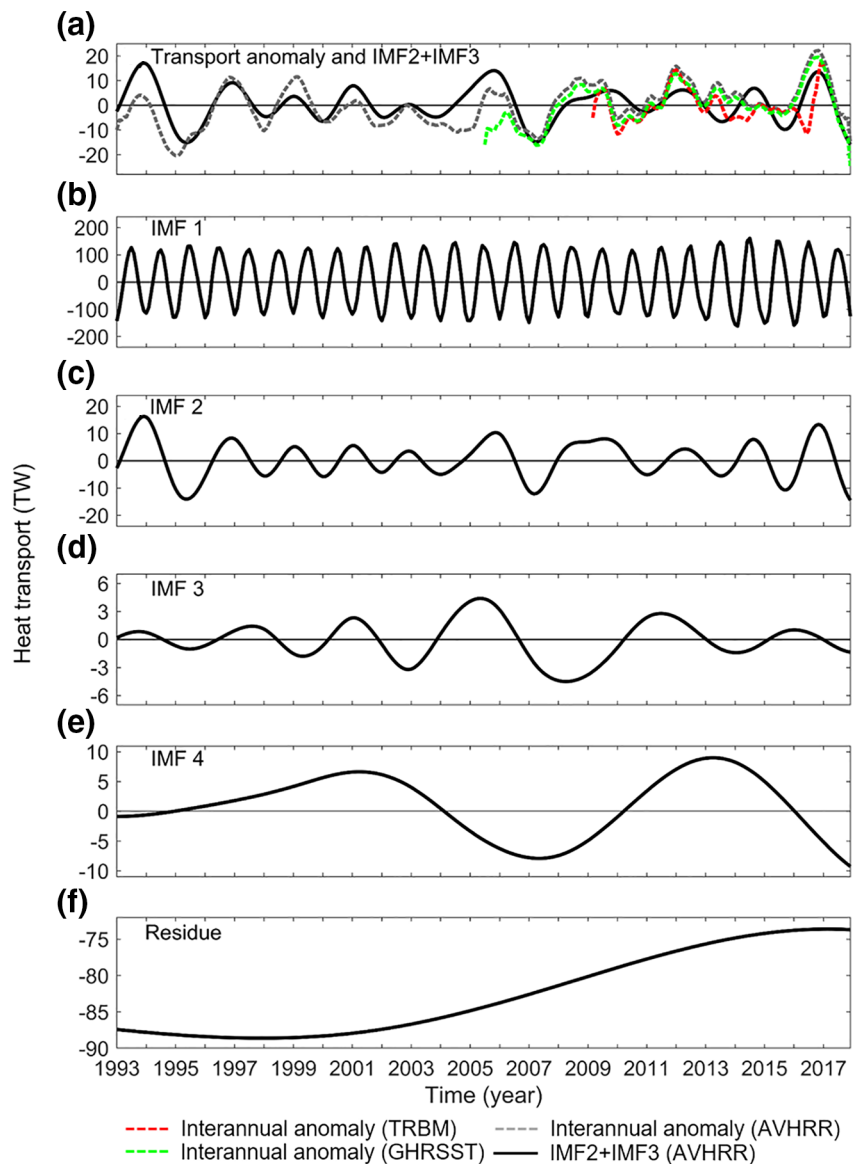


Figure 9. (a) Total heat transport anomalies (dashed lines: red, green, and gray are calculated from CTD, GHRST, and AVHRR, respectively) and IMF2+IMF3 (solid line); (b)–(e) The IMFs of EMD analysis of the total heat transport through the Gaspar and Karimata straits. (f) The residue of the EMD analysis. AVHRR, Advanced Very High Resolution Radiometer; CTD, Conductivity, Temperature, Pressure recorder; EMD, Empirical Mode Decomposition; GHRST, Group for High Resolution Sea Surface Temperature; IMF, Intrinsic Mode Function.

of these four terms are plotted in Figure 12. The results show that both the velocity and salinity anomalies contribute to the interannual variation in the Karimata Throughflow freshwater transport, accounting for approximately 2.34 and 2.98 mSv, respectively (Figure 12b and 12c). Meanwhile, the decreasing trend of southward freshwater transport is explained by both the weakened southward volume transport (~ 0.32 mSv per year) and the salinification (~ 1.26 mSv per year) in the Karimata Strait. $S'V'/S_0$ accounts for an increasing trend of ~ 0.13 mSv per year in southward freshwater transport. It is worth mentioning that the mixed layer salinity in the SCS has shown an increasing trend since 2012, which is attributed to the increasing net surface freshwater loss and horizontal salt advection through the Luzon Strait driven by the SCSTF (Zeng et al., 2018; Zu et al., 2020). This basin-wide salinification in the SCS essentially contributes to the increasing trend of salinity in the Karimata Strait, resulting in reduction of freshwater transport toward the Java Sea.

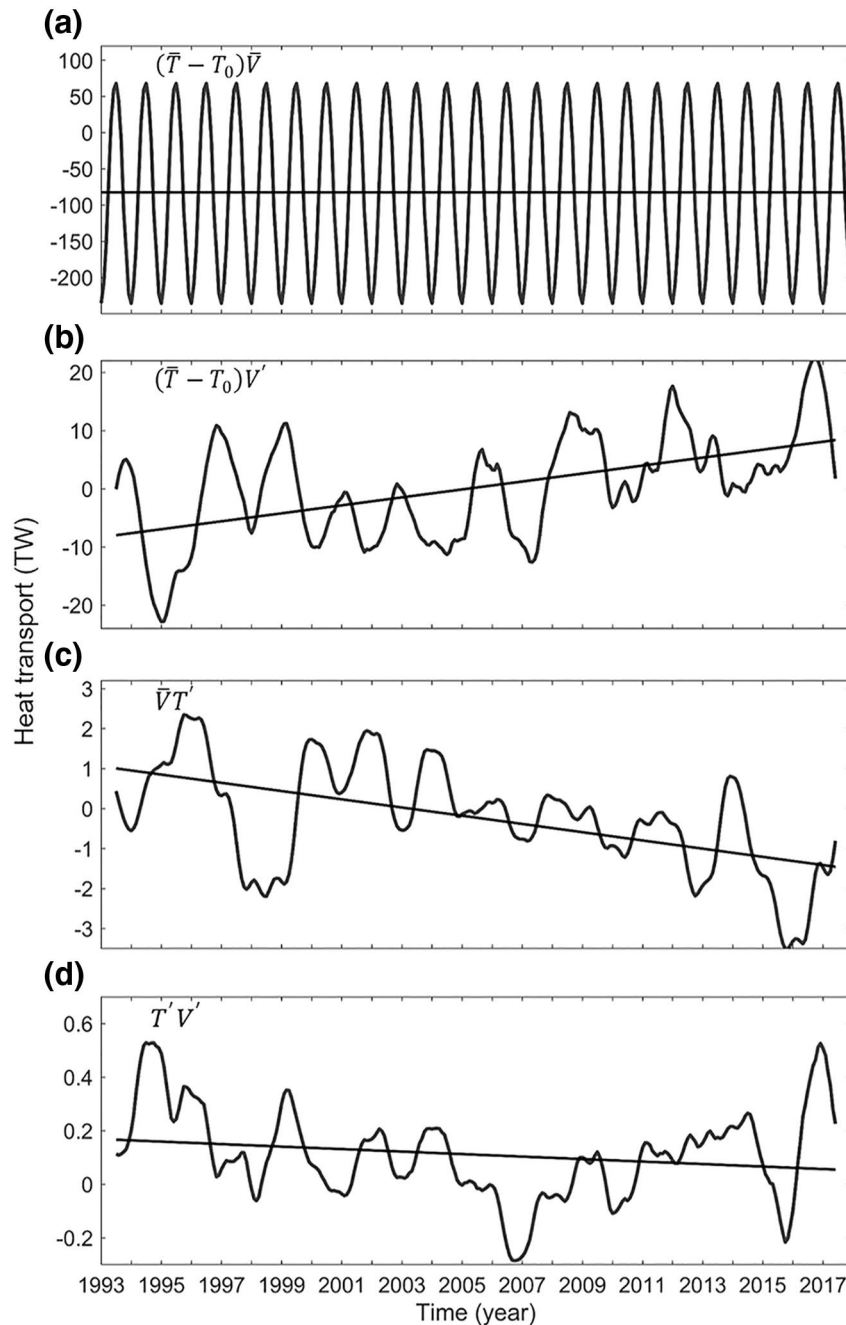


Figure 10. (a) Climatological mean state, (b) current anomaly induced variation, (c) temperature anomaly induced variation, and (d) higher-order terms of the total heat transport of the Karimata Throughflow.

4. Discussion and Conclusions

The Karimata Strait serves as not only an outflow strait of the SCSTF, but also the inflow strait of the ITF (Du et al., 2010). During the northwest monsoon season, the relatively low salinity water in SCS is transported to the Java Sea, and in turn across the Java Sea to join the main route of the ITF in the south of Makassar Strait. According to mooring observations of Gordon et al. (2019), the mean annual cycle of the Makassar Throughflow (0–760 m) shows more volume transport from February to September and less from October to the following January (Figure 13a, also see Figure 4 in Gordon et al., 2019). With a focus on transport in the upper 300 m, the annual cycle of Makassar Throughflow volume transport is basically out of phase with

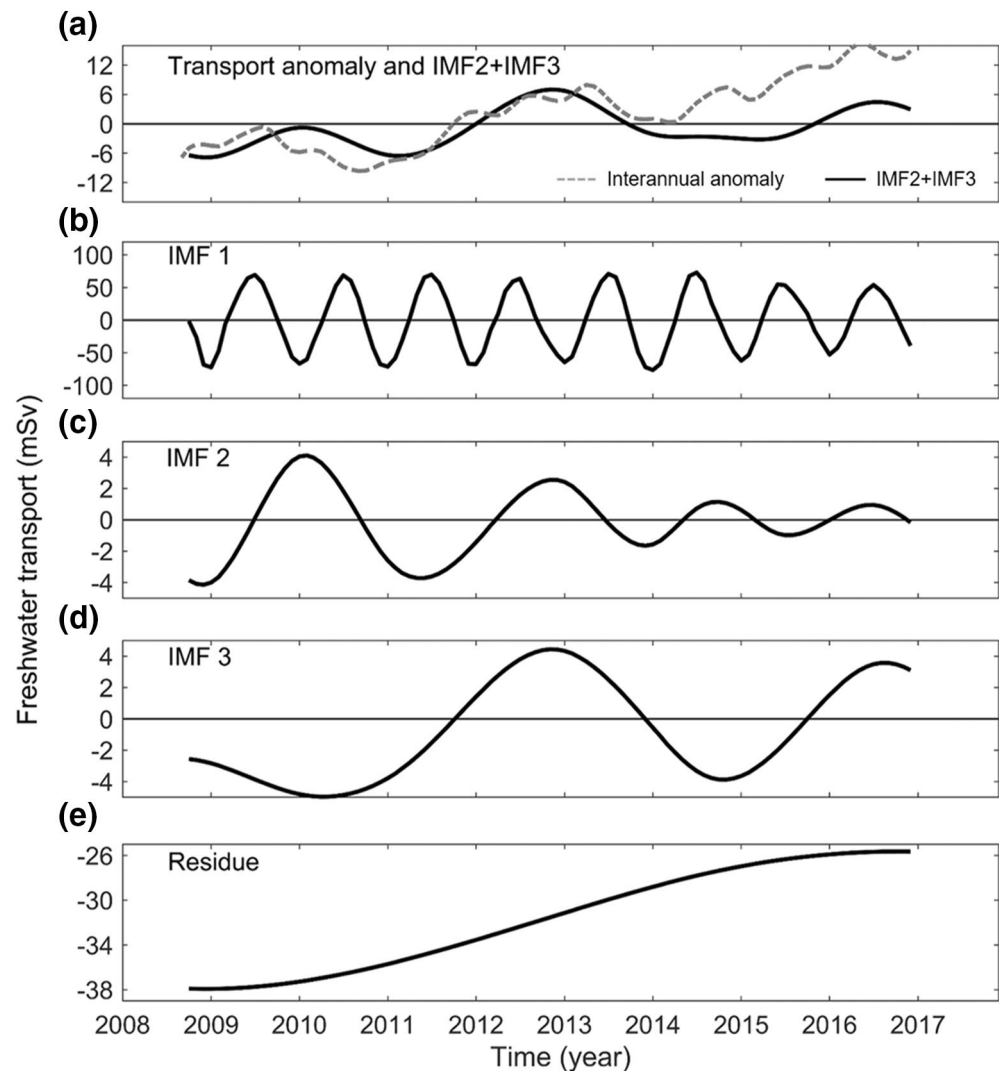


Figure 11. (a) Total freshwater transport anomalies (dashed line) and IMF2+IMF3 (solid line); (b)–(d) The IMFs of EMD analysis of the total freshwater transport through the Gaspar and Karimata straits. (e) The residue of the EMD analysis. EMD, Empirical Mode Decomposition; IMF, Intrinsic Mode Function.

that of Karimata Throughflow (Figure 13a and 13b). The mean volume transport of the Makassar Throughflow in the upper 300 m is -7.23 ± 1.08 Sv from November to the following February. In comparison, the mean volume transport of Karimata Throughflow is -2.22 ± 0.36 Sv during this period. Consequently, the Karimata Throughflow could contribute considerable volume transport, with more than one third of the Makassar Throughflow volume transport during boreal winter. Meanwhile, the Karimata Throughflow carries 209.68 ± 15.19 TW (~ 0.21 PW) of heat flux from the SCS to the Java Sea in boreal winter (Figure 13c). This value is as large as 32% of the averaged estimation of ~ 0.66 PW in the annual mean heat transport of the ITF from different literatures (Hirst & Godfrey, 1993; Vranes, 2002; Tillingier & Gordon, 2010; Xie et al., 2019; Zhang et al., 2019). It should be noted that the ITF heat transport in winter is smaller than its annual mean value, making the contribution of Karimata Throughflow more considerable in winter.

Previous studies suggest a “freshwater plug” effect induced by low salinity water input into the Sulawesi and Java Seas from the SCS through the Mindoro-Sibutu Passage and Karimata Strait, respectively (Fang et al., 2010; Gordon et al., 2012). The input of SCS low salinity surface layer waters builds a pool of buoyant surface water in the northern and southern of the Makassar Strait, that is, the Sulawesi and Flores Seas, which inhibits the southward transport of surface layer waters in the Makassar Strait. This “freshwater

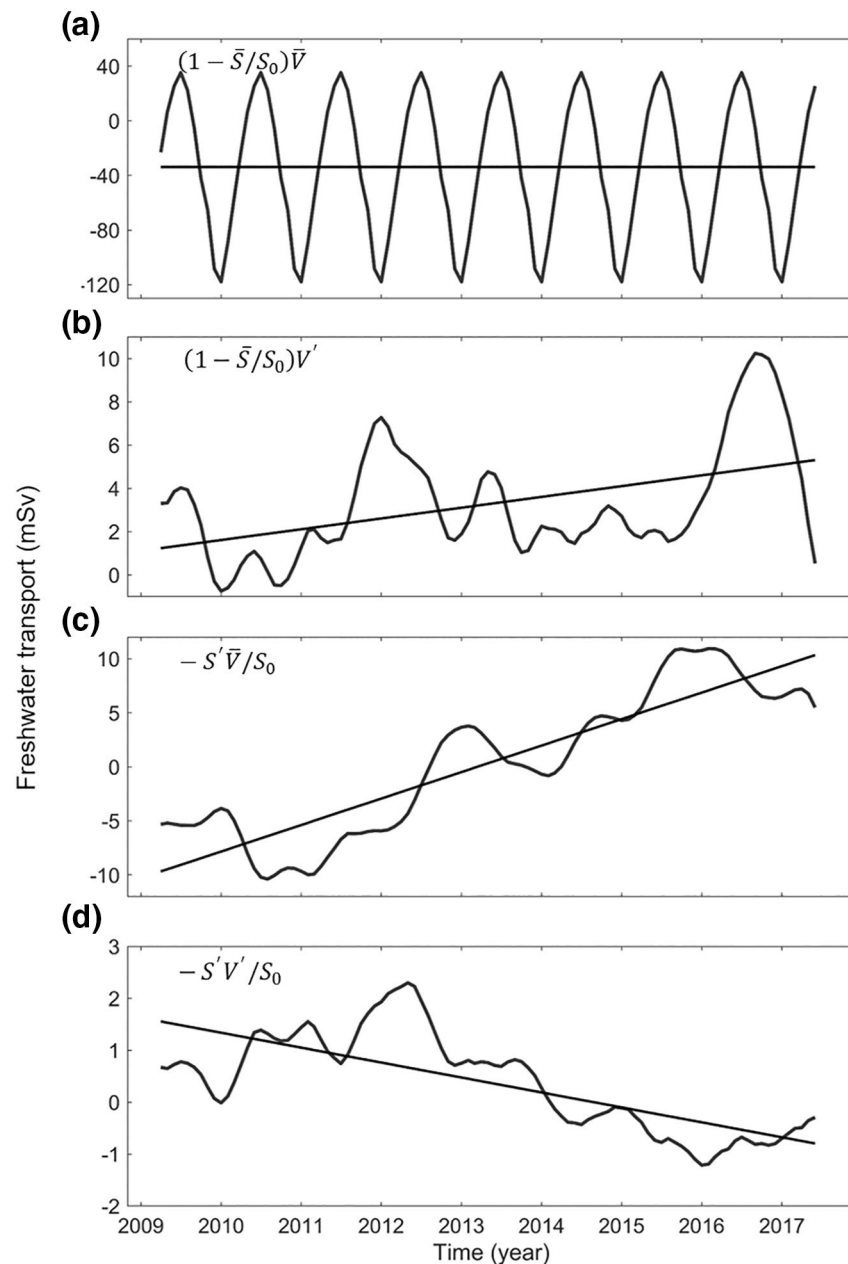


Figure 12. (a) Climatological mean state, (b) current anomaly induced variation, (c) salinity anomaly induced variation, and (d) higher-order term of the total freshwater transport of the Karimata Throughflow.

plug” effect is corroborated by numerical experiments with closing the Karimata Strait and/or the Mindoro-Sibutu Passage (Jiang et al., 2019; Li et al., 2019; Tozuka et al., 2009). Moreover, numerical experiments show that by closing the Karimata Strait only, change in mean ITF volume transport is equivalent to that by closing both the Karimata Strait and Mindoro-Sibutu Passage, suggesting a more critical role of the Karimata Strait for the mean state of ITF transport (Jiang et al., 2019; Li et al., 2019). In the observations, the salinity in Gaspar and Karimata straits is below 34, with a long-term mean value of only 33.09 (Figure 3c), which is at least 0.45 smaller than that in the Mindoro Strait (Sprintall et al., 2012). These limited observations of salinity may partly explain the simulated larger freshwater transport through the Karimata Strait than through the Mindoro Strait, although the Karimata Throughflow volume transport has shown smaller value (Fang et al., 2003; Wang et al., 2019). In this study, we estimate freshwater transport through the Karimata

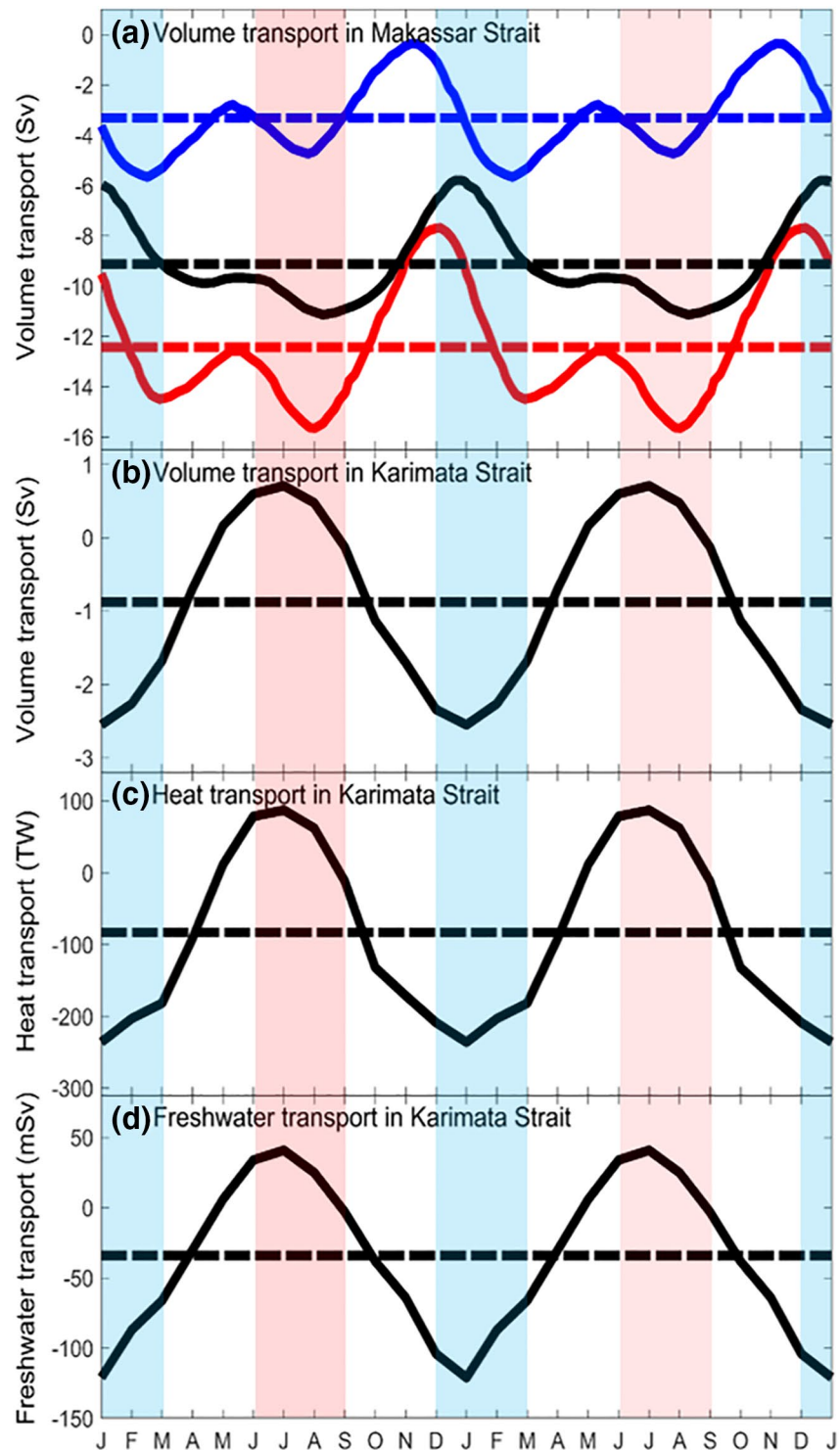


Figure 13. Climatological monthly (a) volume transport of 0–300 m (black), 300–760 m (blue) and 0–760 m (red) in the Makassar Strait; (b) volume, (c) heat and (d) freshwater transports in the Karimata Strait. The dashed lines indicate the annual mean values. The Makassar volume transport data are obtained from Gordon et al. (2019). The peaks of the southeast and northwest monsoons are shaded in magenta and cyan, respectively.

Strait with an annual mean value of -30.87 ± 6.15 mSv. In boreal winter, when the “freshwater plug” effect is active, freshwater transport reaches its peak value of -99.87 ± 15.11 mSv (Figure 13d). Observations from the Tropical Rainfall Measuring Mission (TRMM) show annual mean precipitation of ~ 170 mSv to the

entire Indonesian seas, with a maximum monthly value of ~ 240 mSv occurring from January to February (Kida et al., 2019). Therefore, the Karimata Throughflow freshwater transport, together with the Maritime Continent water cycle, that is, local precipitation and runoff from Kalimantan (Lee et al., 2019), could have a significant impact on the mean state and seasonal variability of ITF transport. Since the Karimata Throughflow transport is subject to strong seasonal reversal features with relatively smaller interannual variation, the water transport through the Mindoro-Sibutu Passage is more crucially important to modulate the ITF in the Makassar Strait on an interannual time scale (Wei et al., 2016).

The volume, heat and freshwater transports seem less correlated with both the IOD and ENSO events (Figure 14). As shown in Figure 14a, the El Niño events during 1993–2017 can be classified as: very strong (1997–1998, 2015–2016), moderate (1994–1995, 2002–2003, and 2009–2010) and weak (2004–2005, 2006–2007, and 2014–2015). The La Niña events are classified as: strong (1998–1999, 1999–2000, 2007–2008, and 2010–2011), moderate (1995–1996 and 2011–2012), and weak (2000–2001, 2005–2006, 2008–2009, and 2016–2017), according to the Oceanic Niño Index (ONI), which is used as the de-facto standard by NOAA (<https://ggweather.com/enso/oni.htm>). The Australian Bureau of Meteorology has identified the positive IOD events in 1994, 1997, 2006, 2012, and 2015, and negative IOD events in 1996, 1998, 2010, 2014, and 2016 (<http://www.bom.gov.au/climate/iod/#tabs=Negative-IOD-impacts>). From Figure 14, it can be seen that the phase of Karimata Throughflow transport could show either in phase, out phase or lag phase with the ONI indices during different periods. For example, during strong El Niño years, the Karimata Throughflow volume transport is in a declining phase in 1997–1998 and is out of phase with the ONI indices between 2015 and 2016, whereas it is in phase with the ONI during the 2002–2003 and 2009–2010 El Niño events. The situation is similar for the relationship between Karimata Throughflow transport and IOD, but with a more implicit complexity since IOD events often co-occur with ENSO events. It is worth mentioning that the El Niño induced basin scale wind and Luzon Strait transport anomalies could effectively modulate the winter circulation in the southern SCS, and thus influence the Mindoro Strait transport (Q. Wang et al., 2020; Zu et al., 2019). However, for the Karimata Strait, the interannual transport anomalies seem to be associated with the maritime continent cross-equatorial flow and the East Asia winter monsoon (Figure 14f and 14g). It should be noted that in the case of freshwater transport, both the current velocity and salinity variations contribute to the interannual anomaly (Figure 12). Of the contribution from the salinity anomaly, it is supposed to be closely related to the East Asia winter monsoon with a similar mechanism as that in the Makassar Strait (Murty et al., 2017).

The annual mean contribution of the Karimata Throughflow volume transport is much smaller than that of the ITF, that is, 0.78 Sv versus 15 Sv. However, the heat and freshwater transport of Karimata Throughflow is considerable, especially in boreal winter. In particular, freshwater transport in winter contributes as much as 42% of the rainfall input to the entire Indonesian seas. Figure 15 shows the transport of volume, heat and freshwater through the Karimata Strait in boreal winter when it directly contributes to the ITF. The results show a significant decreasing trend of southward transport, which can be partly explained by the weakening trend of the maritime continent cross-equatorial flow (Figure 15d). Recently, the so-called “salinity effect” has been proposed to explain the interannual variability and decadal enhancement of the ITF (Hu & Sprintall, 2016, 2017). The results suggest that the halosteric component of the ITF transport contributes approximately $(36 \pm 7)\%$ of the total ITF variability (Hu & Sprintall, 2016). Meanwhile, the intensified rainfall in the Indonesian seas results in a freshening and a subsequent increase in the halosteric component of ITF transport, which is the primary contributor to the decadal enhanced ITF (Hu & Sprintall, 2017). Thus, the reduction in southward freshwater transport through the Karimata Strait would play contradictory roles in the decadal trend of ITF transport: (1) it serves to increase the ITF transport because the “freshwater plug” would be weaker and not inhibit Makassar Throughflow; (2) it would reduce the ITF transport as less freshening of the buoyant plume in the Indo-Australian Basin favoring to weaken the ITF.

5. Summary

Based on direct measurements of current profiles, bottom temperature, salinity, and satellite derived SSS, SST, SSH, and SSW products, we estimated the volume, heat and freshwater transports from the SCS to the Java Sea through the Gaspar and Karimata straits. The Karimata Throughflow is subject to strong seasonal variability, with volume, heat, freshwater transports of -1.98 ± 0.23 Sv, -209.68 ± 15.19 TW,

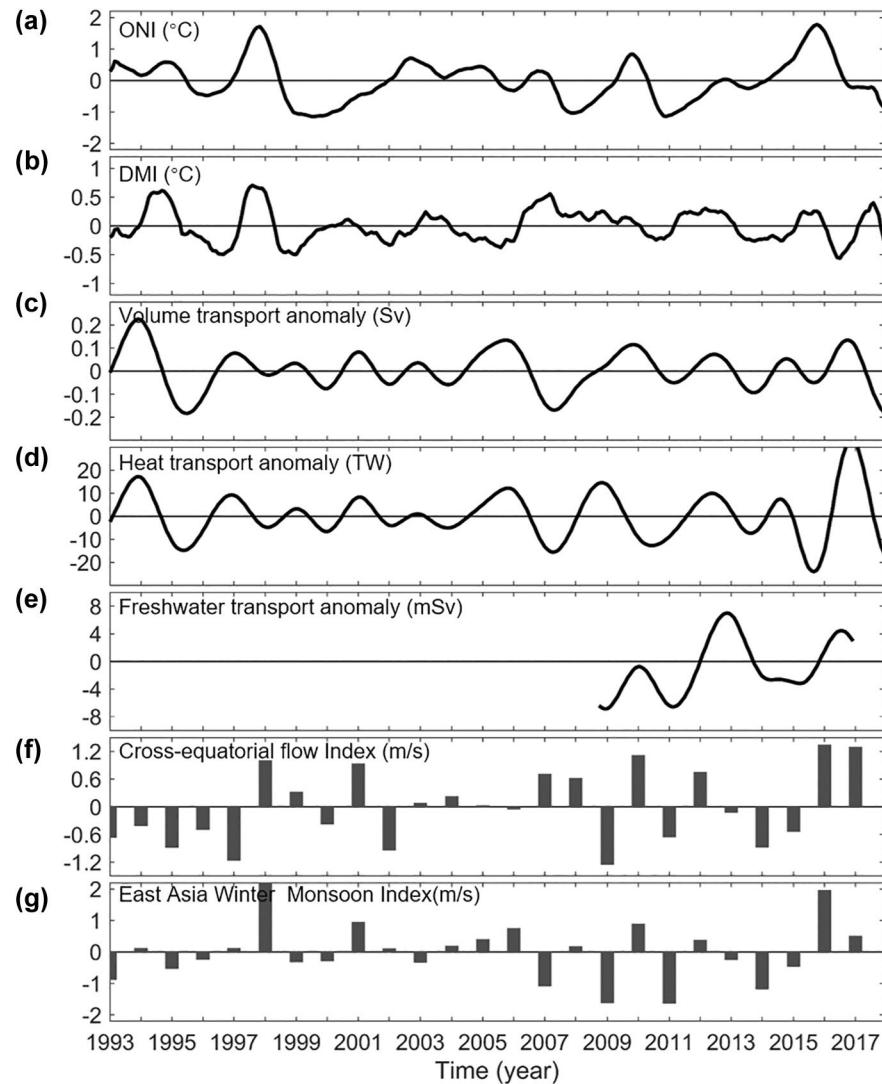


Figure 14. (a) ONI and (b) DMI indices; (c) volume, (d) heat and (e) freshwater transport anomalies of the Karimata Throughflow, (f) cross-equatorial flow indices, and (g) East Asia Winter Monsoon indices over the period of 1993–2017. The time series in (a)–(e) are 13 months running mean smoothed. DMI, Dipole Mode Index; IOD, Indian Ocean Dipole; ONI, Oceanic Niño Index.

–99.87 ± 15.11 mSv in winter, and 0.47 ± 0.20 Sv, 61.06 ± 15.46 TW, 31.67 ± 8.76 mSv in summer, respectively. The annual mean volume, heat and freshwater transports are –0.78 ± 0.12 Sv, –77.31 ± 4.99 TW, and –30.87 ± 6.15 mSv, respectively. Further, we found that the observed ASVs have high correlation with the SSH gradient along the Gaspar and Karimata Straits and the local SSW far beyond the 95% confidence level. A proxy time series of ASV in the Gaspar and Karimata Straits from 1993 to 2017 was developed using SSH gradient and SSW data.

Despite the relatively small annual mean volume transport through the Gaspar and Karimata Straits compared with the ITF, the annual mean heat transport of the Karimata Throughflow contributes considerably, as much as 15% of the ITF. The heat transport of the Karimata Throughflow becomes more important and, roughly equals more than half of the ITF heat transport in boreal winter. Meanwhile, the Karimata Throughflow freshwater transport is as large as 42% of the rainfall input into the entire Indonesian seas in boreal winter. Consequently, the Karimata Throughflow water transport may potentially have an important influence on the Makassar Throughflow in seasonal scale through the “freshwater plug” effect (Fang et al., 2010; Gordon et al., 2012). The hypothesis of the “freshwater plug” is explained by the input of SCS low salinity surface waters to the northern and southern of the Makassar Strait to

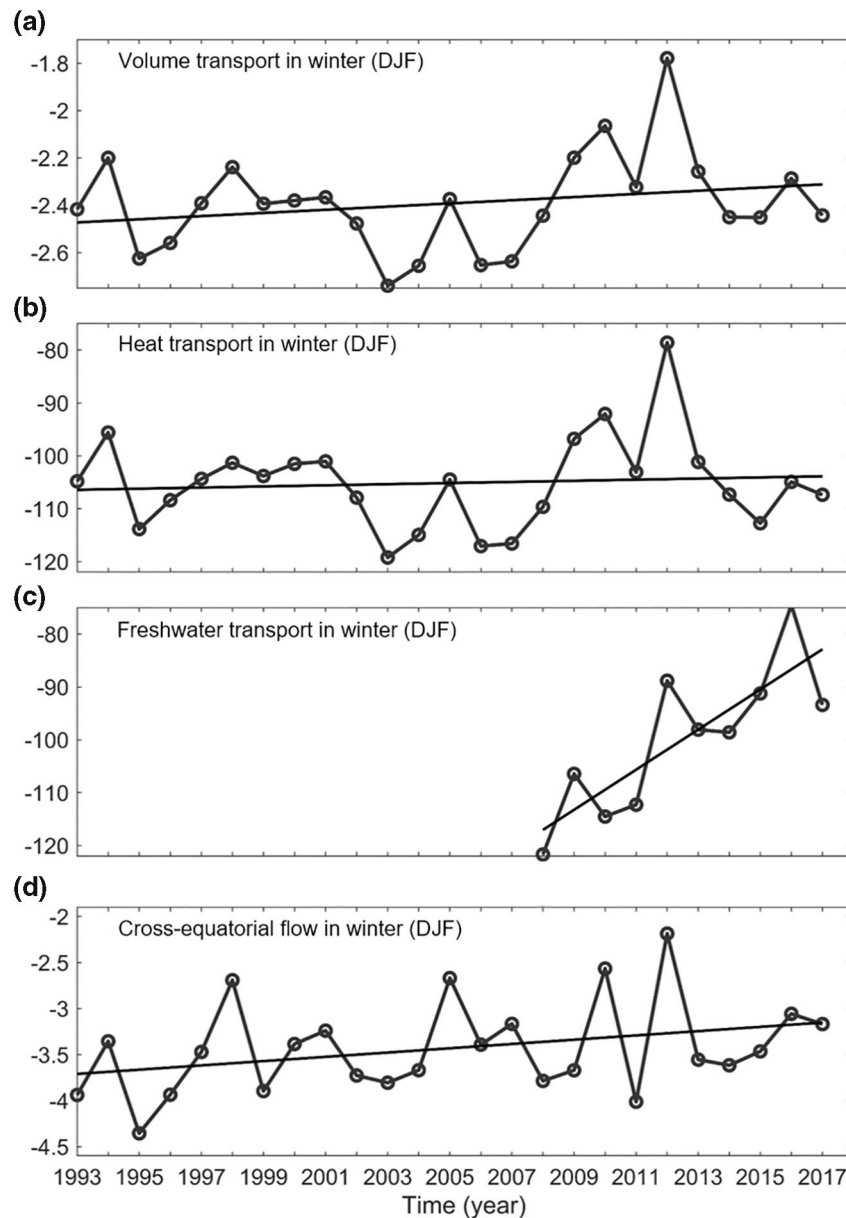


Figure 15. (a) Volume transport, (b) Heat transport, and (c) freshwater transport of the Karimata Throughflow in boreal winter; (d) Cross-equatorial flow index in winter over the period of 1993–2017. Straight lines indicate the trends.

build a pool of buoyant surface water, favoring inhibition of the southward Makassar Throughflow. The “freshwater plug” effect is evidenced by the out-of-phase condition between the seasonal Karimata and Makassar transport (Figure 11) and demonstrated by numerical experiments with blocking related straits (Jiang et al., 2019; Li et al., 2019).

It is interesting that the interannual variability of the Karimata Throughflow shows an insignificant correlation with both the IOD and ENSO indices. In addition, during the period of 1997–2015, the Karimata Throughflow shows a decrease in volume and heat transports of 0.26 Sv and 15 TW from the SCS to the Java Sea, respectively. Freshwater transport has only been available since October 2008, showing a decrease of 12.29 mSv by the end of 2016, equivalent to approximately 33.2%–49.72% of the annual mean freshwater transport over the period of 2009–2016. This decreasing trend may also influence the decadal enhancement of the ITF through the “salinity effect” as suggested by Hu and Sprintall (2017).

Data Availability Statement

The AVHRR SST data are available at https://www.usgs.gov/centers/eros/science/usgs-eros-archive-advanced-very-high-resolution-radiometer-avhrr?qt-science_center_objects=0#qt-science_center_objects. The GHRSSST SST data are available at <https://podaac.jpl.nasa.gov/dataset/UKMO-L4HRfnd-GLOB-OSTIA>. The SMAP SSS data is available at <https://nsidc.org/data/smap/smap-data.html>. The SMOS SSS data are available at <https://www.catds.fr/Products/Available-products-from-CEC-OS/CEC-Ifremer-Dataset-V02>. The AVISO SSH data are available at <http://www.aviso.altimetry.fr/duacs>. The CCMP wind data are available at <http://www.remss.com/measurements/ccmp>. The ERA5 data are available at <https://cds.climate.copernicus.eu/cdsapp#!/dataset/reanalysis-era5-pressure-levels-monthly-means?tab=overview>. The bathymetry ETOPO1 data are available at <http://www.ngdc.noaa.gov/mgg/global>. We appreciate Gordon A.L. for sharing the MITF Makassar data that are available at <https://www.ldeo.columbia.edu/~bhuber/MITF/>. The SITE data are available online <https://github.com/xutengfei0207/SITE/blob/main/SITEDATA.zip>.

Acknowledgments

This study is jointly supported by the National Natural Science Foundation of China (42076023, 41876027, 41821004, 41776042), the MNR Program on Global Change and Air-Sea Interactions (GASI-04-WLHY-03), and the China-Indonesia Maritime Cooperation Fund: Construction of ICCOC and Joint Observation Stations. R. D. Susanto is supported by the US National Science Foundation (OCE-07-25935). We greatly appreciate the captain and the crews of Baruna Jaya IV, I, and VIII for their skillful operation during the voyages and their cooperation in the fieldwork, and we thank all participants in the SITE cruises. We would like to thank the three reviewers for their detailed comments.

References

Atlas, R., Hoffman, R. N., Ardizzone, J., Leidner, S. M., Jusem, J. C., Smith, D. K., & Gombos, D. (2011). A cross-calibrated, multiplatform ocean surface wind velocity product for meteorological and oceanographic applications. *Bulletin of the American Meteorological Society*, 92(2), 157–174. <https://doi.org/10.1175/2010bams2946.1>

Boutin, J., Martin, N., Kolodziejczyk, N., & Reverdin, G. (2016). Interannual anomalies of SMOS sea surface salinity. *Remote Sensing of Environment*, 180, 128–136. <https://doi.org/10.1016/j.rse.2016.02.053>

Boutin, J., Vergely, J. L., Marchand, S., D'Amico, F., Hasson, A., Kolodziejczyk, N., et al. (2018). New SMOS Sea Surface Salinity with reduced systematic errors and improved variability. *Remote Sensing of Environment*, 214, 115–134. <https://doi.org/10.1016/j.rse.2018.05.022>

Broecker, W. S. (1991). The great ocean conveyor. *Oceanography*, 4(2), 79–89. <https://doi.org/10.5670/oceanog.1991.07>

Donlon, C. J., Casey, K. S., Robinson, I. S., Gentemann, C. L., Reynolds, R. W., Barton, I., et al. (2009). The GODAE high-resolution sea surface temperature pilot project. *Oceanography*, 22(3), 34–45. <https://doi.org/10.5670/oceanog.2009.64>

Donlon, C., Robinson, I., Casey, K. S., Vazquez-Cuervo, J., Armstrong, E., Arino, O., et al. (2007). The Global Ocean Data Assimilation experiment high-resolution sea surface temperature pilot project. *Bulletin of the American Meteorological Society*, 88, 1197–1214. <https://doi.org/10.1175/BAMS-88-8-1197>

Ducet, N., Le Traon, P. Y., & Reverdin, G. (2000). Global high-resolution mapping of ocean circulation from TOPEX/Poseidon and ERS-1 and -2. *Journal of Geophysical Research*, 105(C8), 19477–19498. <https://doi.org/10.1029/2000JC900063>

Du, Y., & Qu, T. D. (2010). Three inflow pathways of the Indonesian throughflow as seen from the simple ocean data assimilation. *Dynamics of Atmospheres and Oceans*, 50(2), 233–256. <https://doi.org/10.1016/j.dynatmoce.2010.04.001>

Fang, G. H., Susanto, R. D., Soesilo, I., Zheng, Q. A., Qiao, F. L., & Wei, Z. X. (2005). A note on the South China Sea shallow interocean circulation. *Advances in Atmospheric Sciences*, 22(6), 946–954. <https://doi.org/10.1007/BF02918693>

Fang, G. H., Susanto, R. D., Wirasantosa, S., Qiao, F. L., Supangat, A., Fan, B., et al. (2010). Volume, heat and freshwater transports from the South China Sea to Indonesian seas in the boreal winter of 2007–2008. *Journal of Geophysical Research*, 115(C12), C12020. <https://doi.org/10.1029/2010JC006225>

Fang, G. H., Wang, Y. G., Wei, Z. X., Fang, Y., Qiao, F. L., & Hu, X. M. (2009). Interocean circulation and heat and freshwater budgets of the South China Sea based on a numerical model. *Dynamics of Atmospheres and Oceans*, 47(1–3), 55–72. <https://doi.org/10.1016/j.dynatmoce.2008.09.003>

Fang, G. H., Wei, Z. X., Chio, B. H., Wang, K., Fang, Y., & Wei, L. (2003). Interbasin freshwater, heat and salt transport through the boundaries of the East and South China Seas from a variable-grid global ocean circulation model. *Science in China Series D: Earth Sciences*, 46(2), 149–161. <https://doi.org/10.1360/03yd9014>

Fore, A. G., Yueh, S. H., Tang, W., Stiles, B. W., & Hayashi, A. K. (2016). Combined active/passive retrievals of ocean vector wind and sea surface salinity with SMAP. *IEEE Transactions on Geoscience and Remote Sensing*, 54(12), 7396–7404. <https://doi.org/10.1109/TGRS.2016.2601486>

Gordon, A. L., & Fine, R. A. (1996). Pathways of water between the Pacific and Indian oceans in the Indonesian seas. *Nature*, 379, 146–149. <https://doi.org/10.1038/379146a0>

Gordon, A. L., Huber, B. A., Metzger, E. J., Susanto, R. D., Hurlburt, H. E., & Adi, T. R. (2012). South China Sea throughflow impact on the Indonesian throughflow. *Geophysical Research Letters*, 39(11), L11602. <https://doi.org/10.1029/2012GL052021>

Gordon, A. L., Napitu, A., Huber, B. A., Gruenburg, L. K., Pujiana, K., Agustadi, T., et al. (2019). Makassar Strait Throughflow Seasonal and Interannual Variability: An Overview. *Journal of Geophysical Research: Oceans*, 124(6), 3724–3736. <https://doi.org/10.1029/2018JC014502>

Gordon, A. L., Sprintall, J., Van Aken, H. M., Susanto, R. D., Wijffels, S. E., Molcard, R., et al. (2010). The Indonesian Throughflow during 2004–2006 as observed by the INSTANT program. *Dynamics of Atmospheres and Oceans*, 50(2), 115–128. <https://doi.org/10.1016/j.dynatmoce.2009.12.002>

Gruenburg, L. K., & Gordon, A. L. (2018). Variability in Makassar Strait heat flux and its effect on the eastern tropical Indian Ocean. *Oceanography*, 31(2), 80–87. <https://doi.org/10.5670/oceanog.2018.220>

He, Z. G., Feng, M., Wang, D. X., & Slawinski, D. (2015). Contribution of the Karimata Strait transport to the Indonesian Throughflow as seen from a data assimilation model. *Continental Shelf Research*, 92, 16–22. <https://doi.org/10.1016/j.csr.2014.10.007>

Hersbach, H., Bell, B., Berrisford, P., Hirahara, S., Horányi, A., Muñoz-Sabater, J., et al. (2020). The ERA5 global reanalysis. *Quarterly Journal of the Royal Meteorological Society*, 146, 1999–2049. <https://doi.org/10.1002/qj.3803>

Hirst, A. C., & Godfrey, J. S. (1993). The role of Indonesian throughflow in a global ocean GCM. *Journal of Physical Oceanography*, 23, 1057–1086. [https://doi.org/10.1175/1520-0485\(1993\)023<1057:TROIIT>2.0.CO;2](https://doi.org/10.1175/1520-0485(1993)023<1057:TROIIT>2.0.CO;2)

Huang, N. E., Shen, Z., Long, S. R., Wu, M. C., Shih, H. H., Zheng, Q. A., et al. (1998). The empirical mode decomposition and the Hilbert spectrum for nonlinear and non-stationary time series analysis. *Proceedings of the Royal Society A*, 454, 903–995. <https://doi.org/10.1098/rspa.1998.0193>

- Hu, S. J., & Sprintall, J. (2016). Interannual variability of the Indonesian Throughflow: The salinity effect. *Journal of Geophysical Research: Oceans*, 121(4), 2596–2615. <https://doi.org/10.1002/2015jc011495>
- Hu, S. J., & Sprintall, J. (2017). Observed strengthening of interbasin exchange via the Indonesian seas due to rainfall intensification. *Geophysical Research Letters*, 44(3), 1448–1456. <https://doi.org/10.1002/2016gl072494>
- Jiang, G. Q., Wei, J., Malanotte-Rizzoli, P., Li, M. T., & Gordon, A. L. (2019). Seasonal and Interannual Variability of the Subsurface Velocity Profile of the Indonesian Throughflow at Makassar Strait. *Journal of Geophysical Research: Oceans*, 124, 9644–9657. <https://doi.org/10.1029/2018jc014884>
- Ji, L., & Sun, S. (1997). Model study on the interannual variability of Asia winter monsoon and its influence. *Advances in Atmospheric Sciences*, 14, 1–22. <https://doi.org/10.1007/s00376-997-0039-4>
- Kida, S., Richards, K. J., & Sasaki, H. (2019). The Fate of Surface Freshwater Entering the Indonesian Seas. *Journal of Geophysical Research: Oceans*, 124(5), 3228–3245. <https://doi.org/10.1029/2018jc014707>
- Kolodziejczyk, N., Boutin, J., Vergely, J. L., Marchand, S., Martin, N., & Reverdin, G. (2016). Mitigation of systematic errors in SMOS sea surface salinity. *Remote Sensing of Environment*, 180, 164–177. <https://doi.org/10.1016/j.rse.2016.02.061>
- Lebedev, K. V., & Yaremchuk, M. I. (2000). A diagnostic study of the Indonesian Throughflow. *Journal of Geophysical Research*, 105(C5), 11243–11258. <https://doi.org/10.1029/2000jc900015>
- Lee, T., Fournier, S., Gordon, A. L., & Sprintall, J. (2019). Maritime continent water cycle regulates low-latitude chokepoint of global ocean circulation. *Nature Communications*, 10(2103), 1–13. <https://doi.org/10.1038/s41467-019-10109-z>
- Liu, Q. Y., Feng, M., Wang, D. X., & Wijffels, S. (2015). Interannual variability of the Indonesian Throughflow transport: A revisit based on 30 year expendable bathythermograph data. *Journal of Geophysical Research: Oceans*, 120, 8270–8282. <https://doi.org/10.1002/2015JC011351>
- Liu, Q. Y., Ming, F., & Wang, D. X. (2011). ENSO-induced interannual variability in the southeastern South China Sea. *Journal of Oceanography*, 67(1), 127–133.
- Li, M. T., Wei, J., Wang, D. X., Gordon, A. L., Yang, S., Malanotte-Rizzoli, P., & Jiang, G. Q. (2019). Exploring the Importance of the Mindoro-Sibutu Pathway to the Upper-Layer Circulation of the South China Sea and the Indonesian Throughflow. *Journal of Geophysical Research: Oceans*, 124(7), 5054–5066. <https://doi.org/10.1029/2018jc014910>
- Murty, S. A., Goodkin, N. F., Halide, H., Natawidjaja, D., Suwargadi, B., Suprihanto, I., et al. (2017). Climatic influences on southern Makassar Strait salinity over the past century. *Geophysical Research Letters*, 44(23), 11967–11975. <https://doi.org/10.1002/2017GL075504>
- Qu, T. D., Du, Y., Meyers, G., Ishida, A., & Wang, D. X. (2005). Connecting the tropical Pacific with Indian Ocean through South China Sea. *Geophysical Research Letters*, 32(24), L24609. <https://doi.org/10.1029/2005GL024698>
- Qu, T. D., Du, Y., & Sasaki, H. (2006). South China Sea throughflow: A heat and freshwater conveyor. *Geophysical Research Letters*, 33(23), L23617. <https://doi.org/10.1029/2006GL028350>
- Qu, T. D., Song, T., & Yamagata, T. (2009). An introduction to the South China Sea throughflow: Its dynamics, variability, and implication for climate. *Dynamics of Atmospheres and Oceans*, 47(1–3), 3–14. <https://doi.org/10.1016/j.dynatmoce.2008.05.001>
- Reynolds, R. W., Smith, T. M., Liu, C., Chelton, D. B., Casey, K. S., & Schlax, M. G. (2007). Daily High-Resolution-Blended Analyses for Sea Surface Temperature. *Journal of Climate*, 20(22), 5473–5496. <https://doi.org/10.1175/2007jcli1824.1>
- Saji, N. H., Goswami, B. N., Vinayachandran, P. N., & Yamagata, T. (1999). A dipole mode in the tropical Indian Ocean. *Nature*, 401, 360–363. <https://doi.org/10.1038/43854>
- Sprintall, J., Gordon, A. L., Flament, P., & Villanoy, C. L. (2012). Observations of exchange between the South China Sea and the Sulu Sea. *Journal of Geophysical Research*, 117(C5), C05036. <https://doi.org/10.1029/2011JC007610>
- Sprintall, J., Gordon, A. L., Wijffels, S., Feng, M., Hu, S. J., Koch-Larrouy, A., et al. (2019). Detecting change in the Indonesian Seas. *Frontiers in Marine Science*, 6(257), 1–24. <https://doi.org/10.3389/fmars.2019.00257>
- Sprintall, J., Wijffels, S. E., Molcard, R., & Jaya, I. (2009). Direct estimates of the Indonesian Throughflow entering the Indian Ocean: 2004–2006. *Journal of Geophysical Research*, 114(C7), C07001. <https://doi.org/10.1029/2008JC005257>
- Susanto, R. D., Fang, G. H., Soesilo, I., Zheng, Q. A., Qiao, F. L., Wei, Z. X., & Sulisty, B. (2010). New surveys of a branch of the Indonesian Throughflow. *Eos Transactions AGU*, 91(30), 261–263. <https://doi.org/10.1029/2010EO300002>
- Susanto, R. D., Field, A., Gordon, A. L., & Adi, T. R. (2012). Variability of Indonesian throughflow within Makassar Strait, 2004–2009. *Journal of Geophysical Research*, 117(C9), C09013. <https://doi.org/10.1029/2012JC008096>
- Susanto, R. D., Wei, Z. X., Rameyo, T., Fan, B., Li, S. J., & Fang, G. H. (2013). Observations of the Karimata Strait Throughflow from December 2007 to November 2008. *Acta Oceanologica Sinica*, 32(5), 1–6. <https://doi.org/10.1007/s13131-013-0307-3>
- Talley, L. D. (2013). Closure of the global overturning circulation through the Indian, Pacific, and Southern Oceans: Schematics and transports. *Oceanography*, 26(1), 80–97. <https://doi.org/10.5670/oceanog.2013.07>
- Tillinger, D., & Gordon, A. L. (2010). Transport weighted temperature and internal energy transport of the Indonesian Throughflow. *Dynamics of Atmospheres and Oceans*, 50(2), 224–232. <https://doi.org/10.1016/j.dynatmoce.2010.01.002>
- Torrence, C., & Compo, G. P. (1998). A practical guide to wavelet analysis. *Bulletin of the American Meteorological Society*, 79, 61–78. [https://doi.org/10.1175/1520-0477\(1998\)079<0061:APGTWA>2.0.CO;2](https://doi.org/10.1175/1520-0477(1998)079<0061:APGTWA>2.0.CO;2)
- Tozuka, T., Qu, T. D., Masumoto, & Y., & Yamagata, T. (2009). Impacts of the South China Sea throughflow on seasonal and interannual variations of the Indonesian Throughflow. *Dynamics of Atmospheres and Oceans*, 47(1–3), 73–85. <https://doi.org/10.1016/j.dynatmoce.2008.09.001>
- Tozuka, T., Qu, T. D., & Yamagata, T. (2007). Dramatic impact of the South China Sea on the Indonesian Throughflow. *Geophysical Research Letters*, 34(12), L12612. <https://doi.org/10.1029/2007GL030420>
- Tozuka, T., Qu, T. D., & Yamagata, T. (2015). Impacts of South China Sea Throughflow on El Niño/Southern Oscillation as revealed by a coupled GCM. *Journal of Oceanography*, 71(2), 105–114. <https://doi.org/10.1007/s10872-014-0265-1>
- Vranes, K., Gordon, A. L., & Field, A. (2002). The heat transport of the Indonesian Throughflow and implications for the Indian Ocean heat budget. *Deep Sea Research II*, 49, 1391–1410. [https://doi.org/10.1016/s0967-0645\(01\)00150-3](https://doi.org/10.1016/s0967-0645(01)00150-3)
- Wang, D. X., Liu, Q. Y., Huang, R. X., Du, Y., & Qu, T. D. (2006). Interannual variability of the South China Sea Throughflow inferred from wind data and an ocean data assimilation product. *Geophysical Research Letters*, 33(14), L14605. <https://doi.org/10.1029/2006GL026316>
- Wang, Y., Xu, T. F., Li, S. J., Susanto, R. D., Agustadi, T., Trenggono, M., et al. (2019). Seasonal variation of water transport through the Karimata Strait. *Acta Oceanologica Sinica*, 38(4), 47–57.
- Wang, Q., Zeng, L., Shu, Y., Liu, Q., Zu, T., Li, Y., et al. (2020). Interannual variability of South China Sea winter circulation: response to Luzon Strait transport and El Niño wind. *Climate Dynamics*, 54, 1145–1159. <https://doi.org/10.1007/s00382-019-05050-2>
- Wei, J., Li, M. T., Malanotte-Rizzoli, P., Gordon, A. L., & Wang, D. X. (2016). Opposite Variability of Indonesian Throughflow and South China Sea Throughflow in the Sulawesi Sea. *Journal of Physical Oceanography*, 46(10), 3165–3180. <https://doi.org/10.1175/jpo-d-16-0132.1>

- Wei, Z. X., Li, S. J., Susanto, R. D., Wang, Y. G., Fan, B., Xu, T. F., et al. (2019). An overview of 10-year observation of the South China Sea branch of the Pacific to Indian Ocean throughflow at the Karimata Strait. *Acta Oceanologica Sinica*, 38(4), 1–11. <https://doi.org/10.1007/s13131-019-1410-x>
- Wijffels, S. E., Meyers, G., & Godfrey, J. S. (2008). A 20-yr average of the Indonesian Throughflow: Regional currents and the interbasin exchange. *Journal of Physical Oceanography*, 38, 1965–1978. <https://doi.org/10.1175/2008jpo3987.1>
- Wyrtki, K. (1961). Physical oceanography of the south-east Asian waters. In *Scientific results of marine investigations of the South China Sea and the Gulf of Thailand*, NAGA Report Vol. 2 (p. 195). La Jolla, CA: Scripps Institution of Oceanography.
- Xiao, F., Wang, D., & Yang, L. (2020). Can Tropical Pacific winds enhance the footprint of the interdecadal Pacific Oscillation on the upper-ocean heat content in the South China Sea? *Journal of Climate*, 33, 4419–4437. <https://doi.org/10.1175/JCLI-D-19-0679.1>
- Xiao, F., Wang, D., Zeng, L., Liu, Q. Y., & Zhou, W. (2019). Contrasting changes in the sea surface temperature and upper ocean heat content in the South China Sea during recent decades. *Climate Dynamics*, 53, 1597–1612. <https://doi.org/10.1007/s00382-019-04697-1>
- Xie, T. X., Newton, R., Schlosser, P., Du, C. J., & Dai, M. H. (2019). Long-term mean mass, heat and nutrient flux through the Indonesian Seas, based on the Tritium Inventory in the Pacific and Indian Oceans. *Journal of Geophysical Research: Oceans*, 124(6), 3859–3875. <https://doi.org/10.1029/2018jc014863>
- Xu, D. Y., & Malanotte-Rizzoli, P. (2013). The seasonal variation of the upper layers of the South China Sea (SCS) circulation and the Indonesian through flow (ITF): An ocean model study. *Dynamics of Atmospheres and Oceans*, 63(3), 103–130. <https://doi.org/10.1016/j.dynatmoce.2013.05.002>
- Yaremchuk, M., McCreary, J. P., Yu, Z. J., & Furue, R. (2009). The South China Sea throughflow retrieved from climatological data. *Journal of Physical Oceanography*, 39, 753–767. <https://doi.org/10.1175/2008jpo3955.1>
- Yu, Z., Shen, S., McCreary, J. P., Yaremchuk, M., & Furue, R. (2007). South China Sea throughflow as evidenced by satellite images and numerical experiments. *Geophysical Research Letters*, 34(L01601). <https://doi.org/10.1029/2006GL028103>
- Zeng, L. L., Chassignet, E. P., Schmitt, R. W., Xu, X., & Wang, D. X. (2018). Salinification in the South China Sea since late 2012: Areversal of the freshening since the 1990s. *Geophysical Research Letters*, 45, 2744–2751.
- Zhang, T. C., Wang, W. Q., Xie, Q., & Chen, L. F. (2019). Heat contribution of the Indonesian throughflow to the Indian Ocean. *Acta Oceanologica Sinica*, 38(4), 72–79. <https://doi.org/10.1002/2017GL076574>
- Zeng, L. L., & Wang, D. X. (2009). Intraseasonal variability of latent-heat flux in the South China Sea. *Theoretical and Applied Climatology*, 97, 53–64. <https://doi.org/10.1007/s00704-009-0131-z>
- Zhao, X. X., & Lu, R. Y. (2020). Vertical structure of interannual variability in cross-equatorial flows over the Maritime Continent and Indian Ocean in boreal summer. *Advances in Atmospheric Sciences*, 37(2), 173–186. <https://doi.org/10.1007/s00376-019-9103-0>
- Zu, T. T., Wang, D. X., Wang, Q., Li, M., Wei, J., Geng, B., et al. (2020). A revisit of the interannual variation of the South China Sea upper layer circulation in summer: correlation between the eastward jet and northward branch. *Climate Dynamics*, 54, 457–471. <https://doi.org/10.1007/s00382-019-05007-5>
- Zu, T. T., Xue, H., Wang, D. X., Geng, B., Zeng, L., Liu, Q., et al. (2019). Interannual variation of the South China Sea circulation during winter: Intensified in the southern basin. *Climate Dynamics*, 52, 1917–1933. <https://doi.org/10.1007/s00382-018-4230-3>